THE GEOLOGICAL SOCIETY OF AMERICA®

Recalibrating the Devonian time scale: A new method for integrating radioisotopic and astrochronologic ages in a Bayesian framework

Claire O. Harrigan[1,†], Mark D. Schmitz[1], D. Jeffrey Over[2], Robin B. Trayler[1,3], and Vladimir I. Davydov[1]
[1]*Department of Geosciences, Boise State University, 1910 University Drive, Boise, Idaho 83725, USA*
[2]*Department of Geological Sciences, State University of New York–Geneseo, 1 College Circle, Geneseo, New York 14454, USA*
[3]*Department of Life and Environmental Sciences, University of California–Merced, 5200 Lake Road, Merced, California 95343, USA*

ABSTRACT

The numerous biotic, climatic, and tectonic events of the Devonian cannot be correlated and investigated without a well-calibrated time scale. Here, we updated the calibration of the Devonian time scale using a Bayesian age-depth model that incorporates radioisotopic ages and astrochronology durations. We used existing radioisotopic ages collected and harmonized in the last two geologic time scale compilations, as well as new U-Pb zircon ages from Emsian {Hercules I K-bentonite, Wetteldorf, Germany: 394.290 ± 0.097(0.21)[0.47] Ma} and Eifelian K-bentonites {Tioga B and Tioga F K-bentonites, Fayette, New York, USA: 390.82 ± 0.18(0.26)[0.48] Ma and 390.14 ± 0.14(0.23)[0.47] Ma, respectively}. We anchored floating astrochronology stage durations on radioisotopic ages and chained astrochronologic constraints and uncertainty together to extrapolate conditioning age likelihoods up or down the geologic time scale, which is a new method for integrating astrochronology into age-depth modeling. The modeling results in similar ages and durations for Devonian stages regardless of starting biostratigraphic scaling assumptions. We produced a set of rescaled biostratigraphic zonations, and a new numerical calibration of Devonian stage boundary ages with robust uncertainty estimates, which allow us to evaluate future targets for Devonian time scale research. These methods are broadly applicable for time scale work and provide a template for an integrated stratigraphic approach to time scale modeling.

INTRODUCTION

Our ability to contextualize, correlate, and link significant geologic events and processes depends on the accuracy with which numerical time proxies are integrated into a time scale. Here, we focus on the Devonian Period, wherein numerous studies have investigated the temporal correlation between stratigraphically constrained markers of Devonian biotic crises (House, 2002) and radioisotopically dated causal mechanisms such as meteorite impacts (e.g., Reimold et al., 2005; Gordon et al., 2009) and large igneous provinces (e.g., Ernst et al., 2020). Significant reef expansion and subsequent decline during the Late Devonian is, as of yet, insufficiently explained because of the number of potential causal mechanisms still being explored (Kiessling, 2008; Kiessling and Simpson, 2011, and references therein). Both tectonic factors (e.g., Averbuch et al., 2005) and the expansion and diversification of vascular plants and root systems (e.g., Algeo and Scheckler, 2010), or some combination of the two, have been linked to potential climate effects during the Devonian. Conversely, others have suggested that the evolution of trees was coincident with Devonian climate change, not the cause of climate change (e.g., Retallack and Huang, 2011). In all these cases, to link radioisotopically dated causal mechanisms to events constrained by biostratigraphy, we first need a well-calibrated Devonian time scale. Tectonic, climactic, and biotic factors all interact, and with an improved numerical calibration of the Devonian time scale, we can better understand these interactions. Further, the development of a robust method with which to integrate radioisotopic ages and astrochronology durations can be used to advance chronostratigraphic modeling on any scale.

Numerous efforts (Kaufmann, 2006, and references therein; Becker et al., 2012, 2020; De Vleeschouwer and Parnell, 2014) have sought to refine Devonian stage boundary ages. The fidelity of a chronostratigraphic model for the Devonian depends on three factors: (1) the accuracy and precision of the ages of dated events, (2) the accuracy and precision of the biostratigraphic constraints on those dated events, which provide the correlations and relative stratigraphic positions used in the model, and (3) the method for modeling the relationship between stratigraphic position and age and the fidelity with which the model extrapolates to the age boundaries of interest.

The Devonian global time scale is constructed from a set of conodont biozones that have undergone continued revision in terms of the marker species that are used to define chronostratigraphic units (e.g., Becker et al., 2020, and references therein). To utilize recent improvements in Devonian biostratigraphy and age-depth modeling techniques and to examine those areas in need of further work, an updated numerical calibration of the Devonian time scale is due. Since the compilation of the *Geologic Time Scale 2012* (GTS2012; Gradstein et al., 2012), there have been efforts to redate events with more modern geochronologic techniques (Husson et al., 2016; Lanik et al., 2016; Bodorkos et al., 2017; McAdams et al., 2017; Percival et al., 2018), as well as efforts to find new biostratigraphically constrained, dateable volcanic layers to increase the density of known radioisotopic ages throughout the Devonian (Myrow et al., 2014; Husson et al., 2016; Lanik et al., 2016; Bodorkos et al., 2017). These newly radioisotopically dated volcanic layers have been incorporated into the *Geologic Time Scale 2020* (GTS2020; Gradstein et al., 2020), but the methodology for modeling the numerical age between dated volcanic layers has not been updated for the GTS2020, as discussed further below.

Time scale modeling is often done by fitting age data and relative stratigraphic position data with a model that passes through the data and maintains monotonicity, commonly a linear, spline, or polynomial fit (Telford et al., 2004). Tucker et al. (1998) modeled the Devonian Period with a linear fit by shifting the

Claire O. Harrigan http://orcid.org/0000-0001-9593-7020
[†]claireostwald@u.boisestate.edu.

GSA Bulletin; July/August 2022; v. 134; no. 7/8; p. 1931–1948; https://doi.org/10.1130/B36128.1; 9 figures; 6 tables; 1 supplemental file.
published online 17 November 2021

stratigraphic position of dated volcanic layers until a linear age-depth model was achieved. Similarly, Kaufmann (2006) relied on a linear fit to model the Devonian Period, constructing biostratigraphic scales of conodont biozonation from a composite of stratigraphic sections believed to have continuous deposition. The Devonian chapter of the GTS2012 intentionally discarded the assumption of linearity between age and depth and applied a hybrid spline and linear fit (Becker et al., 2012). However, these types of models typically underestimate uncertainty at positions between radioisotopically dated events (Telford et al., 2004; De Vleeschouwer and Parnell, 2014), which is problematic for time scale calibration, particularly when stage boundaries lack proximal radioisotopically dated volcanic layers. De Vleeschouwer and Parnell (2014) addressed the issue of underestimated model error by applying Bchron, a Bayesian age-depth model (Haslett and Parnell, 2008; Parnell et al., 2008), to the GTS2012 ages for the Devonian Period. Additionally, they supplemented the radioisotopic dates in their model with astrochronologic constraints on the duration of the Frasnian and Givetian Stages as a filter on their posterior model results (De Vleeschouwer et al., 2013a, 2013b; De Vleeschouwer and Parnell, 2014). The GTS2020 compiled new Devonian ages and updated the conodont biostratigraphic chart for the Devonian compared to the GTS2012 but returned to a spline fit through the age and stratigraphic position data (Becker et al., 2020).

Recent developments, including an updated version of the Bchron age-depth model optimized for deep-time Bayesian age modeling (Trayler et al., 2020), newly available radioisotopic ages (this work and references in Becker et al., 2020), and astrochronologic constraints for all but one Devonian stage (House, 1995; Ellwood et al., 2011; De Vleeschouwer et al., 2012, 2015; Ellwood et al., 2015; Da Silva et al., 2016; Whalen et al., 2016; Pas et al., 2018, 2021; Ma et al., 2020), have prompted us to revisit the modeling of the numerical calibration of the Devonian Period. Here, we present new Bayesian age-depth models for the entire Devonian Period and parts of the Silurian and Carboniferous Periods. We applied the methodology to different conodont biozonation schemes to determine the relative scaled stratigraphic positions of our chronological data (radioisotopic ages and astrochronology durations), which we used as model likelihoods. We used the resulting posterior numerical age distributions of the Devonian stage and conodont biozone boundaries to examine how the selection of different biostratigraphic frameworks and their initial scaling assumptions influenced the calibrated time scale ages. We present three Devonian time scales rescaled such that the relative heights of stages and conodont biozones are based on a linear relationship with numerical time.

We also improved the numerical calibration of the Devonian time scale by describing new ages of volcanic layers bracketing the base of the Middle Devonian (Emsian-Eifelian boundary), a section of the Devonian with sparse geochronologic data. We dated three K-bentonites from biostratigraphically well-characterized sedimentary sequences in Wetteldorf, Germany, and Fayette, New York, United States. We leveraged improvements in high-precision U-Pb zircon geochronology by isotope dilution–thermal ionization mass spectrometry (ID-TIMS) over the past couple of decades, namely, the chemical abrasion (CA) technique used to minimize discordance due to Pb loss (Mattinson, 2005), thus improving the accuracy of our ages relative to past attempts to date these K-bentonites.

U-Pb GEOCHRONOLOGY

Sample Descriptions

We targeted K-bentonites in Wetteldorf, Germany, and Fayette, New York, with the aim of improving the accuracy and precision the age of the Emsian-Eifelian boundary. The global stratotype section and point (GSSP) for the base of the Middle Devonian (Emsian-Eifelian boundary) is within the uppermost Heisdorf Formation at Wetteldorf Richtschnitt in the Eifel District of western Germany (Ziegler and Klapper, 1985). The Emsian-Eifelian boundary lies in bed 30 of the uppermost Heisdorf Formation (1.9 m below the base of the Lauch Formation) and corresponds to the first occurrence of the conodont *Polygnathus costatus partitus* in this section (Klapper et al., 1978; Ziegler and Klapper, 1985). Other key conodont taxa in the section at Wetteldorf include *Polygnathus costatus patulus* (Klapper, 1971), the first appearance datum (FAD) of which marks the base of the Emsian *P. c. patulus* zone, and *Polygnathus costatus costatus* (Klapper, 1971), the FAD of which marks the base of the Eifelian *P. c. costatus* zone. The Lower and Middle Devonian strata at Wetteldorf contain numerous K-bentonites (named Hercules, Horologium, Libra, etc.) and well-documented, diverse flora and fauna, inclusive of brachiopods, corals, dacryoconarids, mollusks, ostracodes, trilobites, and spores (Ziegler and Werner, 1982).

Volcanic activity during the Acadian orogeny deposited 80 or more Early to Middle Devonian K-bentonites in the Appalachian Basin (Ver Straeten, 2004). The Emsian-Eifelian boundary in New York State is within the lower Onondaga Formation, which extends from the Hudson Valley to Lake Erie (Ver Straeten, 2007). The Onondaga Formation is primarily limestone with interspersed volcaniclastic layers, including the Tioga set of K-bentonites (Ver Straeten, 2007). The Tioga K-bentonites outcrop throughout the Appalachian Basin and are labeled from oldest to youngest as Tioga A through H (Way et al., 1986), though some areas only contain beds A through G (Ver Straeten, 2004). Ver Straeten (2004) recognized an additional series of up to 32 tephras in the southern Appalachian Basin that are commonly confused with the Tioga A–H beds; he called these 32 tephras the Tioga Middle Coarse Zone cluster.

Correlation of strata in the Onondaga Formation with the Wetteldorf GSSP and recognition of the Emsian-Eifelian boundary in the Onondaga Formation are equivocal due to the absence of diagnostic conodonts and other fauna that might provide correlation in the lower Onondaga Edgecliff Member. The Emsian-Eifelian boundary is conventionally placed at the base of the Onondaga Nedrow Member based on the occurrence of *P. c. partitus* at the Oriskany Falls quarry in Oneida County, New York (Klapper and Oliver, 1995), but the underlying *P. c. patulus* zone has not been recognized, and the boundary could be lower, in the Onondaga Edgecliff Member. In the upper Onondaga Nedrow Member, the FAD of *P. c. costatus* and the co-occurrence of *P. c. patulus* indicate a position low in the *P. c. costatus* zone (Klapper, 1981). Two black shale beds in the upper Onondaga Nedrow Member, associated with dacryoconarids and palynomorphs, indicate the global Chotec event and the base of the *P. c. costatus* zone (Brocke et al., 2016). Two potential ties points between the Wetteldorf GSSP and the Onondaga Formation are the base of the Onondaga Nedrow Member, which is equivocally the base of the *P. c. partitus* zone (Emsian-Eifelian boundary), and the uppermost Onondaga Nedrow Member, which is the base of the *P. c. costatus* zone.

Hercules I K-Bentonite

We sampled the Hercules I K-bentonite from the GSSP section in Wetteldorf, Germany (50.14983°N, 006.47135°E, World Geodetic System 1984 [WGS84]; Fig. 1A). The sampled K-bentonite is 6–7 cm thick, yellow-gray colored, and located above a resistant limestone layer and below a blue-green–colored siltstone. The Hercules I K-bentonite lies within the upper half of the *P. c. costatus* zone (Werner and Winter, 1975; Weddige, 1977, 1982). For the age-depth model described below, this K-bentonite is designated as D13.

In addition to the Hercules I K-bentonite, we also sampled the Hercules II, Horologium I–III, and Libra I–II K-bentonites from the GSSP

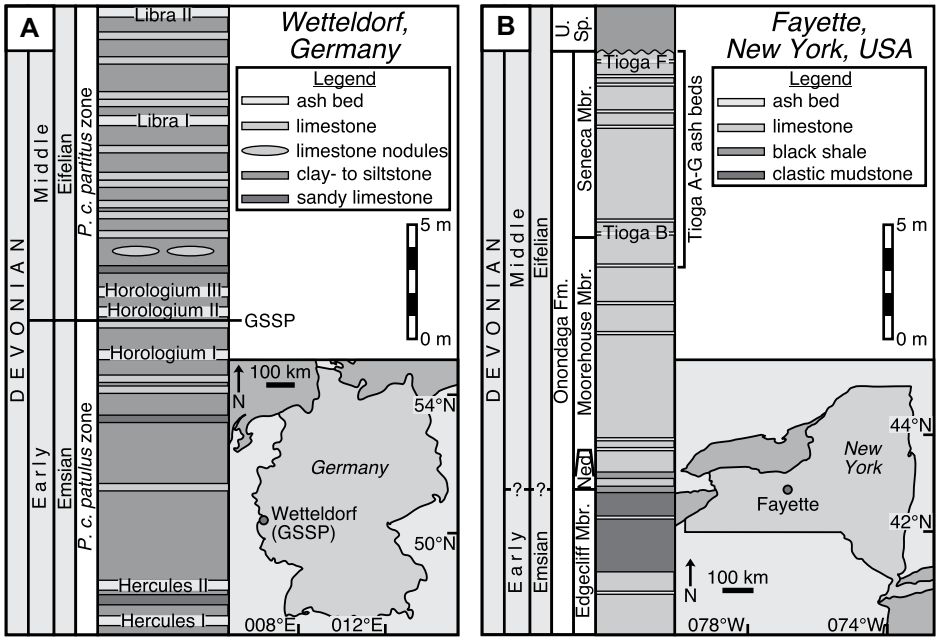

Figure 1. (A) Stratigraphic section for Wetteldorf, Germany, showing location of the Hercules I K-bentonite. Stratigraphic column is modified from Kaufmann et al. (2005). (B) Stratigraphic section for Fayette, New York, showing location of the Tioga B and Tioga F K-bentonites. Stratigraphic column is modified from Ver Straeten (2007). *P. c.—Polygnathus costatus;* GSSP—global stratotype section and point; Fm—Formation; Mbr—Member; Ned—Nedrow Member; U. Sp.—Union Springs Formation.

section in Wetteldorf, Germany (Fig. 1A). Our attempts to date these K-bentonites were unsuccessful because of a combination of inheritance and extreme metamictization of U-rich grains. We discuss, as an example, our CA-ID-TIMS U-Pb zircon dates from the Horologium II K-bentonite in Supplemental Material S1[1] and provide isotopic data for this sample in Supplemental Material S2 (see footnote 1 for all Supplemental Material).

Tioga B K-Bentonite

The Tioga B K-bentonite (Ver Straeten, 2004), also known as the Onondaga Indian Nations bentonite (Brett and Ver Straeten, 1994), outcrops at the Seneca Stone Quarry east of Fayette, New York (42.85462°N, 76.78323°W, WGS84; Fig. 1B). At this location, the Tioga B K-bentonite is ~25 cm thick with a yellow-orange–colored base and a gray-colored, less-altered middle. The upper 5 cm section of the K-bentonite is black and laminated, and we avoided this portion of the bed during sample collection. We interpret the lower 20 cm to represent a single volcanic event despite the internal structure, and we collected a sample that spanned the lower 20 cm of the K-bentonite. The Tioga B K-bentonite defines the upper limit of the Moorehouse Member of the Onondaga Formation (Smith and Way, 1983; Way et al., 1986; Brett and Ver Straeten, 1994; Ver Straeten, 2004) and is placed within the upper half of the *P. c. costatus* zone (Klapper, 1971, 1981). The Tioga B K-bentonite is stratigraphically below the Tioga F K-bentonite. For the age-depth model described below, the Tioga B K-bentonite is designated as D14.

Tioga F K-Bentonite

We also sampled the Tioga F K-bentonite (Ver Straeten, 2004) at the Seneca Stone Quarry (42.85210°N, 76.78977°W, WGS84; Fig. 1B). The Tioga F K-bentonite is ~10 cm thick and gray-black colored, and it appears to be unaltered. The K-bentonite grades from a coarse ash–sized base to a fine ash–sized top. The Tioga F K-bentonite defines the base of the Marcellus Subgroup of the Union Springs Formation (Brett and Ver Straeten, 1994). The Tioga F K-bentonite is assigned to the *Tortodus kockelianus australis* zone (Brett and Ver Straeten, 1994; Ver Straeten, 2007; Klapper, 1981) but could be part of the *P. c. costatus* zone (Klapper, 1981). For the age-depth model described below, the Tioga F K-bentonite is designated as D15.

Previous Geochronology

Hercules I K-Bentonite

The Hercules I K-bentonite at Wetteldorf, Germany, has been dated by Kaufmann et al. (2005). They air-abraded 19 single zircon grains or grain fragments and dated them by ID-TIMS. Cathodoluminescence (CL) images of some zircon grains from the Hercules I K-bentonite revealed inherited cores, while other zircon grains from the same sample exhibited concentric growth zoning. Of the 19 grains, 13 analyses were concordant and yielded $^{206}Pb/^{238}U$ dates ranging from 407.7 to 392.2 Ma. The tips of long prismatic crystals yielded the youngest $^{206}Pb/^{238}U$ dates, ranging from 396.5 to 392.2 Ma. Assuming varying degrees of inheritance in the analyzed grains, Kaufmann et al. (2005) cautiously interpreted the youngest analysis as the age of eruption of the K-bentonite (392.2 ± 1.5 Ma), noting that this date could be biased to a younger age by unrecognized Pb loss.

Several steps can be taken to determine a more robust age for the Hercules I K-bentonite. Since the Kaufmann et al. (2005) study, chemical abrasion has replaced air abrasion as the primary method for mitigating the effects of Pb loss. Chemical abrasion prior to dissolution dissolves the regions of a zircon grain that have been damaged by U radiation and are most susceptible to Pb loss, resulting in more precise and accurate ages (Mattinson, 2005). Additionally, Kaufmann et al. (2005) loaded dissolved zircon directly onto filaments for mass spectrometry without chemical purification. Ion-exchange chromatography separates U and Pb from compounds that may create isobaric interferences or hinder ionization during mass spectrometry (Krogh, 1973). Last, reliance on the weighted mean age of multiple concordant analyses will give a more robust age for the K-bentonite than interpreting a single, youngest date.

Tioga B K-Bentonite

There is one age available for the Tioga B K-bentonite. Roden et al. (1990) dated a sample of the Tioga B K-bentonite from Lewisberg, Union County, Pennsylvania, by ID-TIMS using multigrain monazite fractions and determined a weighted mean $^{207}Pb/^{235}U$ age of 390.0 ± 0.5 Ma. They attempted zircon geochronology but rejected the results due to discordance, which they attributed to inherited Pb in inclusion-rich zircon grains. While monazite

[1]Supplemental Material. Laser ablation–inductively coupled plasma–mass spectrometry (LA-ICP-MS) methods and results, additional age-depth modeling methods, and description of modeling code; LA-ICP-MS data for Hercules I K-bentonite and age-depth model inputs and results; R script for executing age-depth modeling procedure; and R script for anchoring floating astrochronology durations. Please visit https://doi.org/10.1130/GSAB.S.16746136 to access the supplemental material, and contact editing@geosociety.org with any questions.

analyses yielded more concordant results than the zircon analyses, monazite geochronology still has its challenges. Monazite preferentially incorporates Th during crystallization, and thus some of the measured ^{206}Pb must be attributed to the decay of excess ^{230}Th, an intermediate daughter product of ^{238}U, and this consequential excess ^{206}Pb leads to the phenomenon of reverse discordance in monazite. For this reason, Roden et al. (1990) preferred the ^{207}Pb/^{235}U age of the monazite, which is not affected by initial ^{230}Th excess. As with the Hercules I K-bentonite, the geochronology of the Tioga B K-bentonite can be improved through chemical abrasion and ion-exchange chromatography of single zircon grains.

Tioga F K-Bentonite

There has been no previous geochronology of the Tioga F K-bentonite. Tucker et al. (1998) erroneously attributed a ^{207}Pb/^{206}Pb age of 391.4 ± 1.8 Ma to the Tioga F K-bentonite, but according to Ver Straeten (2004), Tucker et al. (1998) actually dated the Tioga Middle Coarse Zone, which is stratigraphically lower than the Tioga A–G K-bentonites. An age for the Eifelian Tioga F K-bentonite will increase the resolution of age-depth models near the Eifelian-Givetian Stage boundary, which is important because the Givetian Stage currently lacks dated volcanic layers that can be used for time scale modeling.

Geochronology Methods

We did all mineral separation, imaging, chemistry, and mass spectrometry at the Boise State University Isotope Geology Laboratory. We separated zircon from all samples using standard magnetic and density separation techniques, and we annealed all zircon at 900 °C for 60 h. We examined 166 zircon grains from the Hercules I K-bentonite by mounting the grains in epoxy, polishing to grain centers, and imaging by cathodoluminescence (CL) in a JEOL T-300 scanning electron microscope with a Gatan MiniCL detector. We placed 59 spots on 47 grains for preliminary ^{206}Pb/^{238}U dating by in situ laser ablation–inductively coupled plasma–mass spectrometry (LA-ICP-MS). See Supplemental Material S1 and S2 for LA-ICP-MS methods and results. We selected zircon grains for CA-ID-TIMS analysis based on oscillatory zoning in CL with no inherited cores and Devonian ^{206}Pb/^{238}U LA-ICP-MS ages (for CL images of selected grains, see Fig. 2). Zircon grains from the Tioga F and Tioga B K-bentonites were too small for mounting, polishing, and LA-ICP-MS analysis, so instead we selected prismatic, needle-like grains in an effort to exclude detrital grains or grains with inherited cores (for photomicrographs of selected grains, see Fig. 2).

We chemically abraded zircon grains selected for high-precision geochronology in a single aggressive step at 190 °C for 12 h, except for grains z1–z8 in the Hercules I K-bentonite sample, which we chemically abraded at 180 °C for 12 h (modified from Mattinson, 2005). We spiked the clean residual grains with the EARTHTIME mixed ^{205}Pb-^{233}U-^{235}U (ET535) tracer solution or the EARTHTIME mixed ^{202}Pb-^{205}Pb-^{233}U-^{235}U (ET2535) tracer solution (Table 1; Condon et al., 2015; McLean et al., 2015). Zircon dissolution and U and Pb separation by ion-exchange chromatography followed the methods described in Davydov et al. (2010).

We took isotopic measurements on an IsotopX GV Isoprobe-T or an IsotopX Phoenix X62 multicollector TIMS with a Daly photomultiplier detector (Pb isotopes as Pb^+) and nine Faraday cups fitted with 10^{12} ohm resistor amplifiers (U isotopes as UO_2^+). We calculated U-Pb ages and uncertainties using the U decay constants of Jaffey et al. (1971) and the algorithms of Schmitz and Schoene (2007). We report uncertainty (2σ) as $\pm X(Y)[Z]$, where X is the internal or analytical uncertainty, Y is the internal and the tracer calibration uncertainty, and Z is the internal, tracer, and decay constant uncertainty.

Geochronology Results

U-Pb zircon CA-ID-TIMS results are shown in Figure 2 (concordia diagrams and ranked date plots with weighted mean ages) and Table 1 (isotopic data and dates for individual grains), described below for each sample, and summarized in Table 2 (weighted mean ages for each sample).

Hercules I K-Bentonite

We dated nine zircon grains from the Hercules I K-bentonite (sample name: 12VD-80) by CA-ID-TIMS. We selected grains based on Devonian LA-ICP-MS age, oscillatory zoning in CL, and elongate, prismatic shape. The nine grains yielded a weighted mean ^{206}Pb/^{238}U age of 394.290 ± 0.097(0.21)[0.47] Ma with a mean square of weighted deviates (MSWD) of 1.6 and a probability of fit of 0.12 (Fig. 2). We interpret this age as the age of eruption and deposition of the Hercules I K-bentonite. Two of the eight grains (z11, z12) were dated using the ET2535 tracer solution, and the ages of these grains are consistent with the ages of the other grains, which were analyzed using the ET535 tracer solution. There is no discernible difference in dates between crystals chemically abraded at 180 °C and those chemically abraded at 190 °C.

Figure 2. Concordia diagrams (left column) and ranked date plots (center column) of U-Pb zircon chemical abrasion–isotope dilution–thermal ionization mass spectrometry (CA-ID-TIMS) results. Error ellipses and error bars are 2σ. Closed symbols are analyses used in weighted mean calculations, and open symbols are analyses excluded from weighted mean calculations. The error on the weighted mean date is reported as a 95% confidence interval on the ranked date plots. The horizontal black band indicates the weighted mean date, the darkest gray horizontal band indicates the internal analytical uncertainty, the medium-gray band incorporates the tracer uncertainty, and the lightest gray band incorporates the decay constant uncertainty. (Right column) Photomicrographs of Tioga F and Tioga B zircon grains and cathodoluminescence images of Hercules I zircon grains. MSWD—mean square of weighted deviates.

Tioga B K-Bentonite

We dated 11 elongate, prismatic zircon grains from the Tioga B K-bentonite (sample name: 2014V27-SSQ-01) by CA-ID-TIMS. Seven of the 11 grains (z2, z5, z3, z6, z8, z13, z4) yielded a weighted mean ^{206}Pb/^{238}U age of 390.82 ± 0.18(0.26)[0.48] Ma with an MSWD of 2.3 and a probability of fit of 0.029, which we interpret as the age of eruption and deposition of the Tioga B K-bentonite (Fig. 2). The four other grains (z18, z11, z9, z20) yielded younger dates, likely because of varying amounts of Pb loss. We dated five of the 11 grains (z9, z11, z13, z18, z20) using the ET2535 tracer solution, and the ages of these grains are consistent with the ages of the other grains, which we analyzed using the ET535 tracer solution.

Tioga F K-Bentonite

We dated 10 elongate, prismatic zircon grains from the Tioga F K-bentonite (sample name: 2014V27-SSQ-02) by CA-ID-TIMS. Of those 10 grains, eight single-grain zircon analyses (z1, z4, z8, z3, z10, z7, z12, z11) yielded a weighted mean ^{206}Pb/^{238}U age of 390.14 ± 0.14(0.23)[0.47] Ma with an MSWD of 3.1 and a probability of fit of 0.0027 (Fig. 2). We rejected the other grains (z5, z6) based on varying amounts of inheritance. We interpret the weighted mean age as the age of eruption and deposition of the Tioga F K-bentonite. We dated four of the 10 grains (z8, z10, z11, z12) using the ET2535 tracer solution, and the ages of these grains are consistent with the ages of the other grains, which we analyzed using the ET535 tracer solution.

Tioga F

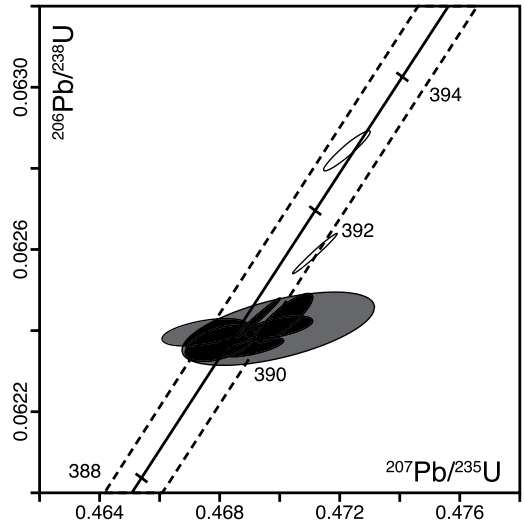

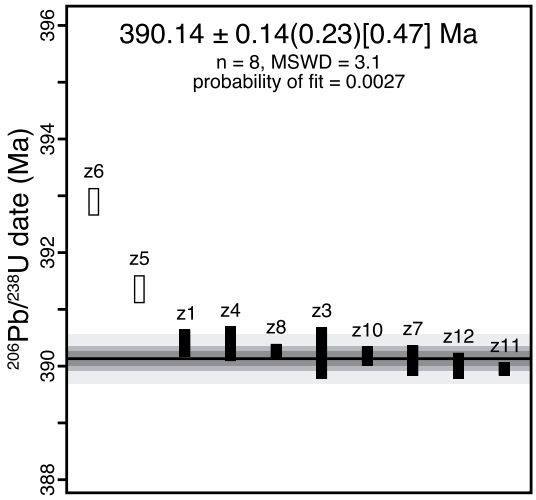

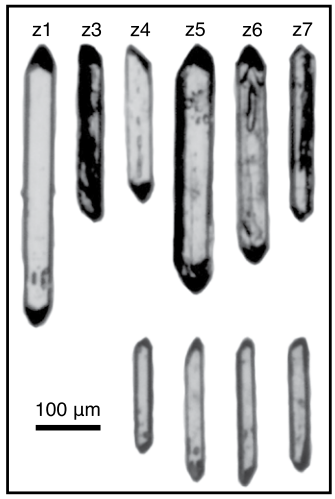

Tioga B

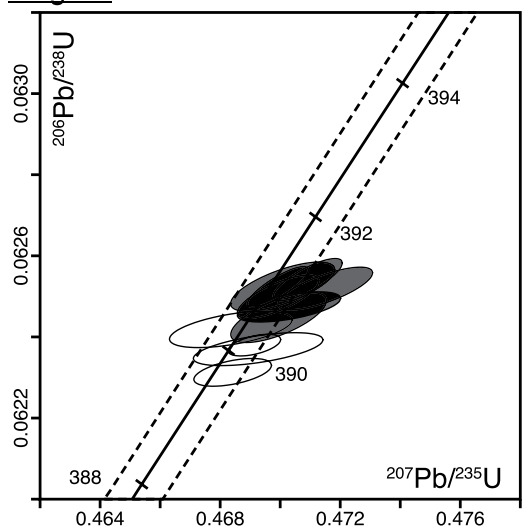

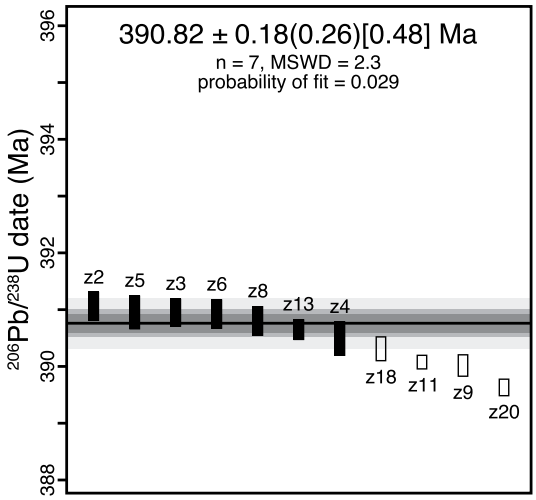

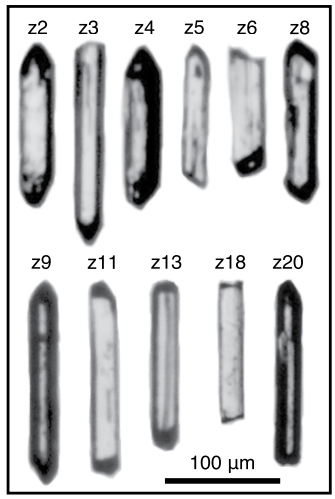

Hercules I

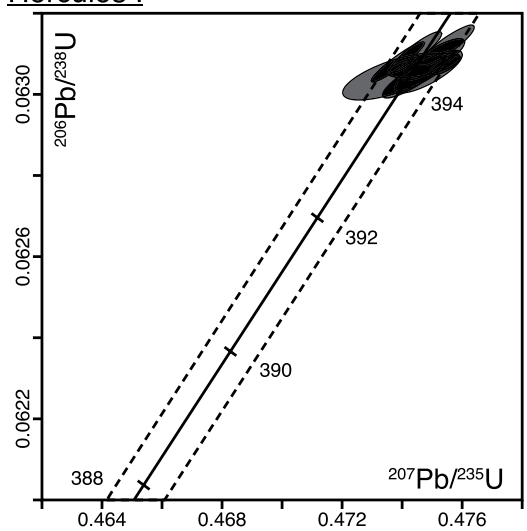

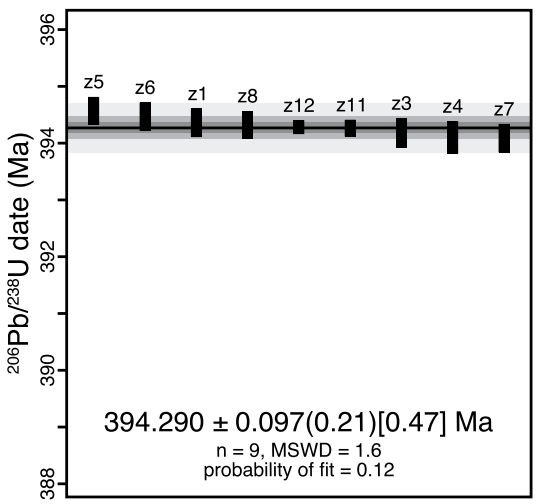

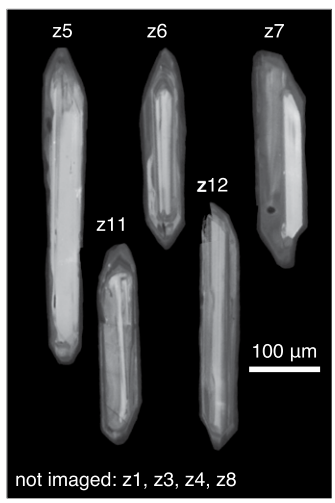

TABLE 1. U-Pb ZIRCON ISOTOPIC DATA AND AGES OF INDIVIDUAL GRAINS

Sample†	Spike§	Compositional parameters						Radiogenic isotope ratios								Isotopic ages					
		Th/U#	$^{206}Pb^{*}$†† ($\times10^{-13}$ mol)	$^{206}Pb^{*}$†† (mol %)	Pb^{*}/Pb_c††	Pb_c†† (pg)	$^{206}Pb/^{204}Pb$§§	$^{208}Pb/^{206}Pb$##	$^{207}Pb/^{206}Pb$##	% err†††	$^{207}Pb/^{235}U$##	% err†††	$^{206}Pb/^{238}U$##	% err†††	Corr. coef.§§§	$^{207}Pb/^{206}Pb$### (Ma)	±††† (Ma)	$^{207}Pb/^{235}U$### (Ma)	±††† (Ma)	$^{206}Pb/^{238}U$### (Ma)	±††† (Ma)
Tioga F (2014V27-SSQ-02)																					
z6	ET535	0.182	2.6696	99.82%	150	0.41	9811	0.0574	0.054500	0.078	0.47223	0.135	0.062842	0.064	0.943	391.77	1.75	392.73	0.44	392.89	0.24
z5	ET535	0.103	6.2586	99.80%	136	1.03	9155	0.0325	0.054596	0.066	0.47115	0.129	0.062589	0.065	0.986	395.71	1.48	391.98	0.42	391.35	0.25
z1	**ET535**	**0.113**	**6.7774**	**99.89%**	**236**	**0.65**	**15750**	**0.0357**	**0.054515**	**0.066**	**0.46928**	**0.127**	**0.062433**	**0.063**	**0.977**	**392.38**	**1.48**	**390.69**	**0.41**	**390.40**	**0.24**
z4	**ET535**	**0.185**	**1.5237**	**99.61%**	**71**	**0.49**	**4674**	**0.0583**	**0.054615**	**0.109**	**0.47012**	**0.166**	**0.062431**	**0.080**	**0.838**	**396.48**	**2.43**	**391.27**	**0.54**	**390.39**	**0.30**
z8	**ET2535**	**0.288**	**0.7550**	**99.11%**	**32**	**0.56**	**2027**	**0.0906**	**0.054615**	**0.180**	**0.46995**	**0.199**	**0.062409**	**0.036**	**0.569**	**396.48**	**4.04**	**391.16**	**0.64**	**390.26**	**0.14**
z3	**ET535**	**0.066**	**0.3016**	**98.06%**	**14**	**0.49**	**932**	**0.0209**	**0.054615**	**0.498**	**0.46993**	**0.558**	**0.062405**	**0.119**	**0.584**	**396.50**	**11.17**	**391.14**	**1.81**	**390.23**	**0.45**
z10	**ET2535**	**0.159**	**0.6892**	**98.87%**	**24**	**0.65**	**1602**	**0.0500**	**0.054339**	**0.235**	**0.46748**	**0.253**	**0.062395**	**0.044**	**0.494**	**385.14**	**5.27**	**389.45**	**0.82**	**390.17**	**0.17**
z7	**ET535**	**0.221**	**1.1056**	**98.64%**	**20**	**1.26**	**1334**	**0.0697**	**0.054409**	**0.171**	**0.46799**	**0.221**	**0.062383**	**0.071**	**0.787**	**388.00**	**3.83**	**389.80**	**0.72**	**390.10**	**0.27**
z12	**ET2535**	**0.272**	**0.7876**	**99.32%**	**41**	**0.45**	**2641**	**0.0859**	**0.054421**	**0.183**	**0.46799**	**0.205**	**0.062369**	**0.059**	**0.495**	**388.53**	**4.11**	**389.80**	**0.66**	**390.01**	**0.22**
z11	**ET2535**	**0.283**	**0.7579**	**99.31%**	**41**	**0.44**	**2613**	**0.0890**	**0.054557**	**0.161**	**0.46909**	**0.180**	**0.062359**	**0.031**	**0.676**	**394.12**	**3.61**	**390.56**	**0.58**	**389.96**	**0.12**
Tioga B (2014V27-SSQ-01)																					
z2	**ET535**	**0.196**	**0.9581**	**99.26%**	**37**	**0.59**	**2437**	**0.0618**	**0.054610**	**0.151**	**0.47091**	**0.199**	**0.062541**	**0.068**	**0.794**	**396.31**	**3.39**	**391.82**	**0.65**	**391.06**	**0.26**
z5	**ET535**	**0.230**	**0.5704**	**98.37%**	**17**	**0.79**	**1106**	**0.0724**	**0.054529**	**0.253**	**0.47008**	**0.302**	**0.062524**	**0.079**	**0.693**	**392.96**	**5.68**	**391.25**	**0.98**	**390.96**	**0.30**
z3	**ET535**	**0.255**	**1.1943**	**99.45%**	**51**	**0.55**	**3259**	**0.0802**	**0.054511**	**0.127**	**0.46992**	**0.177**	**0.062523**	**0.065**	**0.836**	**392.21**	**2.86**	**391.13**	**0.57**	**390.95**	**0.25**
z6	**ET535**	**0.172**	**0.6975**	**98.67%**	**20**	**0.78**	**1362**	**0.0541**	**0.054697**	**0.227**	**0.47150**	**0.273**	**0.062519**	**0.069**	**0.739**	**399.87**	**5.09**	**392.22**	**0.89**	**390.93**	**0.26**
z8	**ET535**	**0.355**	**0.7171**	**99.14%**	**33**	**0.52**	**2103**	**0.1117**	**0.054532**	**0.190**	**0.46993**	**0.236**	**0.062499**	**0.069**	**0.740**	**393.11**	**4.27**	**391.14**	**0.77**	**390.81**	**0.26**
z13	**ET2535**	**0.291**	**0.5114**	**99.02%**	**29**	**0.42**	**1838**	**0.0917**	**0.054597**	**0.275**	**0.47029**	**0.299**	**0.062474**	**0.049**	**0.566**	**395.75**	**6.16**	**391.39**	**0.97**	**390.65**	**0.18**
z4	**ET535**	**0.305**	**0.6323**	**98.89%**	**25**	**0.59**	**1625**	**0.0959**	**0.054579**	**0.230**	**0.46994**	**0.277**	**0.062448**	**0.081**	**0.679**	**395.03**	**5.16**	**391.15**	**0.90**	**390.49**	**0.31**
z18	ET2535	0.411	0.3893	97.72%	13	0.75	791	0.1293	0.054420	0.329	0.46835	0.357	0.062418	0.059	0.532	388.47	7.39	390.05	1.15	390.32	0.22
z11	ET2535	0.377	1.0173	99.39%	48	0.52	2971	0.1185	0.054545	0.138	0.46913	0.153	0.062380	0.035	0.518	393.61	3.10	390.59	0.50	390.08	0.13
z9	ET2535	0.221	0.4290	98.60%	20	0.50	1290	0.0696	0.054568	0.349	0.46926	0.376	0.062370	0.053	0.567	394.58	7.82	390.68	1.22	390.02	0.20
z20	ET2535	0.420	0.6458	98.74%	23	0.68	1435	0.1323	0.054519	0.206	0.46841	0.225	0.062313	0.045	0.507	392.54	4.63	390.09	0.73	389.68	0.17
Hercules I (12VD-80)																					
z5	**ET535**	**1.070**	**1.8731**	**99.69%**	**113**	**0.48**	**5909**	**0.3368**	**0.054638**	**0.098**	**0.47551**	**0.151**	**0.063119**	**0.064**	**0.890**	**397.44**	**2.20**	**394.99**	**0.49**	**394.57**	**0.25**
z6	**ET535**	**1.066**	**1.1925**	**99.70%**	**117**	**0.29**	**6108**	**0.3353**	**0.054531**	**0.095**	**0.47445**	**0.149**	**0.063102**	**0.065**	**0.903**	**393.03**	**2.12**	**394.26**	**0.49**	**394.47**	**0.25**
z1	**ET535**	**0.834**	**0.8937**	**99.55%**	**73**	**0.33**	**4054**	**0.2625**	**0.054615**	**0.129**	**0.47505**	**0.178**	**0.063085**	**0.066**	**0.832**	**396.49**	**2.88**	**394.67**	**0.58**	**394.36**	**0.25**
z8	**ET535**	**1.044**	**1.3286**	**99.61%**	**88**	**0.43**	**4653**	**0.3286**	**0.054483**	**0.096**	**0.47385**	**0.154**	**0.063078**	**0.064**	**0.939**	**391.07**	**2.16**	**393.85**	**0.50**	**394.32**	**0.24**
z12	**ET2535**	**1.276**	**1.7298**	**99.68%**	**111**	**0.47**	**5565**	**0.4015**	**0.054671**	**0.066**	**0.47544**	**0.085**	**0.063072**	**0.032**	**0.721**	**398.78**	**1.47**	**394.94**	**0.28**	**394.28**	**0.12**
z11	**ET2535**	**0.698**	**0.8935**	**98.95%**	**30**	**0.79**	**1725**	**0.2195**	**0.054589**	**0.186**	**0.47470**	**0.206**	**0.063069**	**0.038**	**0.570**	**395.41**	**4.18**	**394.43**	**0.67**	**394.26**	**0.15**
z3	**ET535**	**0.631**	**0.7858**	**99.49%**	**61**	**0.33**	**3532**	**0.1985**	**0.054622**	**0.146**	**0.47488**	**0.193**	**0.063055**	**0.068**	**0.793**	**396.77**	**3.27**	**394.55**	**0.63**	**394.18**	**0.26**
z4	**ET535**	**0.841**	**0.4685**	**98.88%**	**29**	**0.44**	**1608**	**0.2647**	**0.054503**	**0.255**	**0.47376**	**0.301**	**0.063043**	**0.075**	**0.688**	**391.88**	**5.73**	**393.78**	**0.98**	**394.10**	**0.28**
z7	**ET535**	**1.349**	**1.3601**	**99.27%**	**50**	**0.83**	**2462**	**0.4246**	**0.054575**	**0.126**	**0.47437**	**0.177**	**0.063040**	**0.065**	**0.859**	**394.86**	**2.82**	**394.20**	**0.58**	**394.09**	**0.25**

†z1, z2, etc., are labels for single zircon grains or fragments annealed and chemically abraded after Mattinson (2005). Samples and their corresponding values in bold were used in the weighted mean age calculation.

§Samples were spiked with the EARTHTIME mixed ^{205}Pb-^{233}U-^{235}U (ET535) tracer solution or the EARTHTIME mixed ^{202}Pb-^{205}Pb-^{233}U-^{235}U (ET2535) tracer solution (Condon et al., 2015; McLean et al., 2015).

#Model Th/U ratio iteratively calculated from the radiogenic $^{208}Pb/^{206}Pb$ ratio and $^{206}Pb/^{238}U$ age.

††Pb^{*} and Pb_c represent radiogenic and common Pb, respectively; mol % $^{206}Pb^{*}$ is given with respect to radiogenic, blank, and initial common Pb.

§§Measured ratio corrected for spike and fractionation only. Fractionation was estimated at 0.18 ± 0.03%/a.m.u. for Daly analyses, based on analysis of NBS-981 and NBS-982.

##Corrected for fractionation, spike, and common Pb; up to 1 pg of common Pb was assumed to be procedural blank: $^{206}Pb/^{204}Pb = 18.042\% \pm 0.61\%$; $^{207}Pb/^{204}Pb = 15.537\% \pm 0.52\%$; $^{208}Pb/^{204}Pb = 37.686\% \pm 0.63\%$ (all uncertainties 1σ). Excess over blank was assigned to initial common Pb, using the Stacey and Kramers (1975) two-stage Pb isotope evolution model at the nominal sample age.

†††Errors are 2σ, propagated using the algorithms of Schmitz and Schoene (2007).

§§§Corr. coef.—correlation coefficient.

###Calculations are based on the decay constants of Jaffey et al. (1971). The $^{206}Pb/^{238}U$ and $^{207}Pb/^{206}Pb$ ages were corrected for initial disequilibrium in $^{230}Th/^{238}U$ using $Th/U_{(magma)} = 3$.

TABLE 2. SUMMARY OF U-Pb ZIRCON SAMPLE AGES

K-bentonite (sample number)	$^{206}Pb/^{238}U$ weighted mean age* (Ma)	MSWD†	Prob. of fit§	*n*#
Fayette, New York, USA				
Tioga F (2014V27-SSQ-02)	390.14 ± 0.14(0.23)[0.47]	3.1	0.0027	8
Tioga B (2014V27-SSQ-01)	390.82 ± 0.18(0.26)[0.48]	2.3	0.029	7
Wetteldorf, Germany				
Hercules I (12VD-80)	394.290 ± 0.097(0.21)[0.47]	1.6	0.12	9

*All weighted mean ages are at the 95% confidence interval, as calculated from the internal 2σ errors. Uncertainties are quoted as ± *X*(*Y*)[*Z*], where *X* is the internal or analytical uncertainty, *Y* is the uncertainty including the tracer calibration, and *Z* includes the decay constant uncertainty.
†MSWD—mean square of weighted deviation.
§Prob. of fit—probability of fit.
#*n*—number of analyses included in weighted mean.

AGE-DEPTH MODELING

Modeling Methods

We used the modifiedBChron R package (Trayler et al., 2020) to create Bayesian age-depth models of the Devonian using likelihood functions based upon the radioisotopic ages of biostratigraphically constrained events and astrochronologic constraints on Devonian stage durations. Although we were not explicitly modeling in the accumulative stratal depth domain, the biostratigraphic position in a time scale is the product of an accumulative (evolutionary) process with stochastic variability in the number of events and accumulation rates, and thus we posit that the underling mathematical models of Bayesian age-depth modeling are applicable. While we retain the term "age-depth" modeling for its simplicity, the reader is asked to intuit the identity of depth as the relative distance measure of the rock bodies that comprise a chronostratigraphic scale. The "age-depth" models we produced allowed us to determine the age and uncertainty of stratigraphic positions between dated events, specifically stage and conodont biozone boundaries.

Our model inputs were based on radioisotopic ages, biostratigraphic constraints on dated events, and astrochronology stage durations. We investigated how varying relative stratigraphic position of radioisotopic ages influenced the resulting age-depth model by creating a model for three different published conodont biozonation schemes. We incorporated 28 radioisotopic ages into our models (Table 3). We incorporated astrochronologic constraints (Table 4) on the duration of Devonian stages by anchoring an astrochronology duration constraint on a radioisotopic age.

We ran models in R (R Core Team, 2021) using the input parameters listed in Tables 3 and 5, using 10,000 iterations (following burn-in) of a Markov chain Monte Carlo simulation to produce the highest density interval that modeled the relationship between age and depth. Age-depth model inputs and results are available in Supplemental Material S2, and code for executing the model is available as Supplemental Material S3.

From the model output, we determined stage and conodont biozone boundary ages and uncertainties. To create time-linear biostratigraphic time scales where the relative intervals of the biostratigraphic scale are directly correlative to

TABLE 3. MODEL LIKELIHOODS: RADIOISOTOPIC AGES

Identifier	Age* (Ma)	Reference	Tracer	Model likelihood, age† (Ma)	Scaled stratigraphic position§		
					Kaufmann (2006) scale	Becker et al. (2012) scale	Becker et al. (2020) scale
Cb2	358.43 ± 0.06(0.19)[0.42]	Davydov et al. (2011)	ET535 or ET2535	358.43 ± 0.06	101.32 ± 0.78	102.93 ± 0.83	101.76 ± 0.44
Cb1	358.71 ± 0.06(0.19)[0.42]	Davydov et al. (2011)	ET2535	358.71 ± 0.06	100.27 ± 0.27	101.05 ± 1.05	100.66 ± 0.66
D27	358.89 ± 0.20(0.29)[0.48]	Myrow et al. (2014)	ET535	358.89 ± 0.20	98.97 ± 1.02	99.19 ± 0.81	98.96 ± 0.35
D26	358.97 ± 0.11(0.19)[0.43]	Myrow et al. (2014)	ET535	358.97 ± 0.11	98.97 ± 1.02	99.19 ± 0.81	98.21 ± 0.39
D25	359.25 ± 0.06(0.18)[0.42]	Davydov et al. (2011)	ET535 or ET2535	359.25 ± 0.06	98.97 ± 1.02	99.19 ± 0.81	97.82 ± 0.79
D23	363.4 ± 1.8	Tucker et al. (1998)	In-house	362.87 ± 0.53	95.73 ± 0.68	97.37 ± 1.01	95.25 ± 0.59
D22	363.8 ± 2.2	Tucker et al. (1998)	In-house	364.08 ± 2.05	95.73 ± 0.68	97.37 ± 1.01	95.25 ± 0.59
D19	372.360 ± 0.053(0.11)[0.41]	Percival et al. (2018)	ET2535	372.360 ± 0.053	71.40 ± 1.03	75.05 ± 1.45	78.76 ± 0.48
D18	375.14 ± 0.12(0.22)[0.45]	Lanik et al. (2016)	ET535 or ET2535	375.14 ± 0.12	63.81 ± 0.37	67.76 ± 0.98	73.90 ± 0.46
D17	375.25 ± 0.13(0.22)[0.45]	Lanik et al. (2016)	ET535 or ET2535	375.25 ± 0.13	64.62 ± 0.43	67.76 ± 0.98	74.75 ± 0.39
D16	375.55 ± 0.10(0.21)[0.44]	Lanik et al. (2016)	ET535 or ET2535	375.55 ± 0.10	63.72 ± 1.32	67.76 ± 0.98	74.75 ± 0.39
D15	390.14 ± 0.14(0.23)[0.47]	This work	ET535 or ET2535	390.14 ± 0.14	49.89 ± 0.97	48.66 ± 0.99	48.37 ± 2.77
D14	390.82 ± 0.18(0.26)[0.48]	This work	ET535 or ET2535	390.82 ± 0.18	49.63 ± 0.72	48.66 ± 0.99	47.41 ± 1.81
D13	394.290 ± 0.097(0.21)[0.47]	This work	ET535 or ET2535	394.290 ± 0.097	44.73 ± 1.01	42.47 ± 0.52	40.83 ± 0.55
D12	407.7 ± 0.7	Kaufmann et al. (2005)	In-house	407.75 ± 1.08	21.62 ± 1.21	23.77 ± 2.10	24.34 ± 0.70
D11	411.7 ± 0.9	Bodorkos et al. (2017)	Not described	411.7 ± 0.9	12.94 ± 2.78	16.63 ± 2.66	12.64 ± 1.58
D10	411.5 ± 1.1(1.2)[1.3]	Parry et al. (2011)	Not described	411.5 ± 1.2	17.23 ± 5.05	19.24 ± 4.34	12.64 ± 1.58
D9	415.6 ± 0.8	Bodorkos et al. (2017)	Not described	415.6 ± 0.8	4.04 ± 2.63	6.95 ± 3.79	3.00 ± 3.00
D8	417.7 ± 0.5	Bodorkos et al. (2017)	Not described	417.7 ± 0.5	1.74 ± 2.47	3.84 ± 3.84	3.00 ± 3.00
D7	417.22 ± 0.21(0.23)[0.50]	Husson et al. (2016)	ET535 or ET2535	417.22 ± 0.21	4.38 ± 1.52	8.28 ± 2.46	3.39 ± 1.13
D6	417.61 ± 0.12(0.23)[0.50]	McAdams et al. (2017)	ET535	417.61 ± 0.12	4.38 ± 1.52	8.28 ± 2.46	3.39 ± 1.13
D5	417.68 ± 0.21(0.27)[0.52]	Husson et al. (2016)	ET535 or ET2535	417.68 ± 0.21	4.38 ± 1.52	8.28 ± 2.46	3.39 ± 1.13
D4	417.56 ± 0.20(0.26)[0.51]	Husson et al. (2016)	ET535 or ET2535	417.56 ± 0.20	4.38 ± 1.52	8.28 ± 2.46	3.39 ± 1.13
D3	417.73 ± 0.22(0.28)[0.53]	Husson et al. (2016)	ET535 or ET2535	417.73 ± 0.22	4.38 ± 1.52	8.28 ± 2.46	3.39 ± 1.13
D2	417.85 ± 0.23(0.29)[0.54]	Husson et al. (2016)	ET535 or ET2535	417.85 ± 0.23	4.38 ± 1.52	8.28 ± 2.46	3.39 ± 1.13
D1	418.42 ± 0.21(0.27)[0.53]	Husson et al. (2016)	ET535 or ET2535	418.42 ± 0.21	4.38 ± 1.52	8.28 ± 2.46	3.39 ± 1.13
S8	422.91 ± 0.07(0.21)[0.49]	Cramer et al. (2014)	ET535	422.91 ± 0.07	-4.62 ± 0.40	-6.31 ± 0.65	-6.11 ± 0.72
S7	424.08 ± 0.20(0.29)[0.53]	Cramer et al. (2014)	ET535	424.08 ± 0.20	-6.49 ± 0.49	-9.33 ± 0.80	-8.76 ± 0.68

*Ages are from the listed references, except for D12, D22, and D23, which have been recalculated by Schmitz (2012). When available, we show 2σ uncertainty as ± *X*(*Y*)[*Z*], where *X* is the analytical uncertainty, *Y* is the uncertainty including the tracer calibration, and *Z* includes the decay constant uncertainty.
†For samples dated using an EARTHTIME tracer (Condon et al., 2015; McLean et al., 2015), we used the analytical uncertainty in our modeling. If the tracer was in-house or unknown, we used the uncertainty including the tracer calibration. Age uncertainty is 2σ.
§The units of scaled stratigraphic position are relative to the Silurian-Devonian boundary set equal to 0 and the Devonian-Carboniferous boundary set equal to 100. The uncertainty on scaled stratigraphic position is expressed as ± the half width.

TABLE 4. ASTROCHRONOLOGIC CONSTRAINTS

Duration (m.y.)	Reported uncertainty sources	Reference	Revised uncertainty* (m.y.)	Reasons for revised uncertainty*	Combined duration* (m.y.)
Famennian					
13.5 ± 0.5	Stratigraphic uncertainty on stage boundaries + 1 cycle counting error	Pas et al. (2018)	N.A.†	N.A.	13.82 ± 0.16
14.40 ± 0.28	Stratigraphic uncertainty on stage boundaries	Ma et al. (2020)	±0.68	Added one 405 k.y. counting error	
Frasnian					
6.7 ± 0.4	1 cycle counting error	De Vleeschouwer et al. (2012); Whalen et al. (2016)	±0.50	Added one 100 k.y. uncertainty to account for stratigraphic uncertainty on stage boundaries	6.7 ± 0.5
Givetian					
6.5	Not reported	House (1995)	±1.95	Arbitrary 30% uncertainty on duration estimate to account for counting error and uncertainty on precession period	4.91 ± 0.35
5.6	Not reported	Ellwood et al. (2011)	±1.10	Two 405 k.y. cycles counting error + three 100 k.y. stratigraphic uncertainty on composite construction	
4.35 ± 0.45	Stratigraphic uncertainty on stage boundaries + 1 cycle counting error	De Vleeschouwer et al. (2015)	±0.75	Added three 100 k.y. stratigraphic uncertainty on composite construction	
Eifelian					
6.28	Not reported	Ellwood et al. (2015)	±1.00	Two 405 k.y. cycle counting error + two 100 k.y. stratigraphic uncertainty on composite construction	5.50 ± 0.39
5	Not reported	Pas et al. (2021)	±0.80	One 405 k.y. cycle counting error + two 200 k.y. uncertainty to account for stratigraphic uncertainty on stage boundaries	
Pragian					
1.7 ± 0.7	Stratigraphic uncertainty on stage boundaries + 1 cycle counting error	Da Silva et al. (2016)	N.A.	N.A.	1.7 ± 0.7
Lochkovian					
7.7 ± 2.8	Stratigraphic uncertainty on stage boundaries + 6 cycle counting error	Da Silva et al. (2016)	N.A.	N.A.	7.7 ± 2.8

*This study.
†N.A.—not applicable.

numerical time, we adjusted the stratigraphic positions of stage and conodont biozones boundaries such that the Bayesian posterior median was linearized between the Silurian-Devonian and Devonian-Carboniferous boundaries. This essentially stretched portions of the time scale for which the scaled stratigraphic position (*y* axis) increased at a lesser rate than the passage of numerical time (*x* axis) and compressed portions of the time scale for which numerical time increased less rapidly than the relative time represented by the scaled stratigraphic position. This created linearized time scales with stage and conodont biozone scaling informed by numerical time and allowed us to assess how strongly different initial conodont biozonation schemes influenced the results of the modeling.

Starting Conodont Biozonation Schemes

We created three age-depth models based on three different conodont biozonation schemes to understand how the initial construction of the biostratigraphic scale influenced the final model results. Hereafter, "Kaufmann scale" refers to the alternative and standard conodont biostratigraphic scales of Kaufmann (2006). The term "Becker 2012 scale" refers to the conodont biozones of the GTS2012 (Becker et al., 2012). The term "Becker 2020 scale" refers to the conodont biozones from the GTS2020 (Becker et al., 2020). The three conodont biozonation schemes and relative scales are documented in Figure 3.

Importantly, the Kaufmann and Becker biostratigraphic scales were constructed with contrasting fundamental assumptions in zonal scaling. The Kaufmann scale is a composite scale of nine well-characterized sections from around the world, and the scale was constructed under the assumption that those sections had constant stratal accumulation rates. The relative durations of biozones are thus linked to lithostratigraphic thickness. Conversely, the Becker scales were initially built upon the implicit assumption of equal biozone durations, although subsequent calibration exercises in successive Geologic Time Scale volumes (House and Gradstein, 2004; Becker et al., 2012, 2020) have modulated this starting assumption. Neither starting assumption is fully realistic, and these assumptions can be examined, and their resultant scales modified, through the use of age modeling that can stretch and compress the duration of stages and biozones pulled from these existing scales. The emphasis on scaffolding and modifying the Devonian time scale based on radioisotopic ages is present in the work by Kaufmann (2006) and Becker et al. (2012, 2020) and continues here.

We projected the three starting scales to the same normalized interval such that position 0 indicates the Silurian-Devonian boundary and position 100 indicates the Devonian-Carboniferous boundary. This allowed us to directly compare the scales, particularly in terms of the numerical ages of stage boundaries that resulted from the modeling.

Radioisotopic Age Constraints for Model

We used 24 $^{206}Pb/^{238}U$ zircon ages from this work and the Devonian chapter of the GTS2020 (Becker et al., 2020, and references therein), two U-Pb zircon ages from the Silurian chapter of the GTS2020 (Melchin et al., 2020, and references therein), and two U-Pb zircon ages from the Carboniferous chapter of the GTS2020 (Aretz et al., 2020, and references therein), and we assigned those ages to a scaled stratigraphic position for our modeling (Fig. 3; Table 3). We included Silurian and Carboniferous ages in our models to minimize uncertainty caused by the model extrapolating across the Silurian-Devonian and Devonian-Carboniferous boundaries. Generally, we accepted the conodont biozone assignment from the references that published each age, and we assigned a scaled stratigraphic position to each age for each scale based on that conodont biozone assignment.

TABLE 5. MODEL LIKELIHOODS: ASTROCHRONOLOGIC CONSTRAINTS

Identifier	Anchor			Model likelihood, age* (Ma)			Scaled stratigraphic position†		
	Identifier	Radiometric age (Ma)	Reference	Kaufmann (2006) scale	Becker et al. (2012) scale	Becker et al. (2020) scale	Kaufmann (2006) scale	Becker et al. (2012) scale	Becker et al. (2020) scale
A-baseFamennian-D27	D27	358.89 ± 0.20	Myrow et al. (2014)	372.71 ± 0.27	372.71 ± 0.27	372.71 ± 0.27	73.19 ± 1.02	77.88 ± 0.81	80.23 ± 0.69
A-baseFrasnian-D27	D27	358.89 ± 0.20	Myrow et al. (2014)	379.41 ± 0.64	379.41 ± 0.64	379.41 ± 0.64	59.78 ± 1.02	60.54 ± 0.81	67.17 ± 0.69
A-baseGivetian-D27	D27	358.89 ± 0.20	Myrow et al. (2014)	384.32 ± 0.76	384.32 ± 0.76	384.32 ± 0.76	52.42 ± 1.02	52.19 ± 0.81	56.45 ± 0.69
A-baseEifelian-D27	D27	358.89 ± 0.20	Myrow et al. (2014)	389.82 ± 0.88	389.82 ± 0.88	389.82 ± 0.88	45.74 ± 1.02	43.03 ± 0.81	41.37 ± 0.69
A-baseCarboniferous-D15	D15	390.14 ± 0.14	This paper	363.36 ± 0.78	363.36 ± 0.78	363.36 ± 0.78	100.00 ± 0.50	100.00 ± 0.50	100.00 ± 0.50
A-baseFamennian-D15	D15	390.14 ± 0.14	This paper	377.18 ± 0.76	377.18 ± 0.76	377.18 ± 0.76	73.19 ± 0.50	77.88 ± 0.50	80.23 ± 0.50
A-baseFrasnian-D15	D15	390.14 ± 0.14	This paper	383.88 ± 0.50	383.88 ± 0.50	383.88 ± 0.50	59.78 ± 0.50	60.54 ± 0.50	67.17 ± 0.50
A-baseGivetian-D15	D15	390.14 ± 0.14	This paper	388.79 ± 0.29	388.79 ± 0.29	388.79 ± 0.29	52.42 ± 0.50	52.19 ± 0.50	56.45 ± 0.50
A-D15	D15	390.14 ± 0.14	This paper	390.14 ± 0.14	390.14 ± 0.14	390.14 ± 0.14	50.61 ± 0.50	49.71 ± 0.50	52.36 ± 0.50
A-baseEifelian-D15	D15	390.14 ± 0.14	This paper	393.79 ± 0.69	393.79 ± 0.69	393.79 ± 0.69	45.74 ± 0.50	43.03 ± 0.50	41.37 ± 0.50
A-baseCarboniferous-D14	D14	390.82 ± 0.18	This paper	362.43 ± 0.92	362.43 ± 0.92	362.43 ± 0.92	100.00 ± 0.50	100.00 ± 0.50	100.00 ± 0.50
A-baseFamennian-D14	D14	390.82 ± 0.18	This paper	376.25 ± 0.91	376.25 ± 0.91	376.25 ± 0.91	73.19 ± 0.50	77.88 ± 0.50	80.23 ± 0.50
A-baseFrasnian-D14	D14	390.82 ± 0.18	This paper	382.95 ± 0.70	382.95 ± 0.70	382.95 ± 0.70	59.78 ± 0.50	60.54 ± 0.50	67.17 ± 0.50
A-baseGivetian-D14	D14	390.82 ± 0.18	This paper	387.86 ± 0.57	387.86 ± 0.57	387.86 ± 0.57	52.42 ± 0.50	52.19 ± 0.50	56.45 ± 0.50
A-D14	D14	390.82 ± 0.18	This paper	390.82 ± 0.18	390.82 ± 0.18	390.82 ± 0.18	48.47 ± 0.50	46.77 ± 0.50	47.53 ± 0.50
A-baseEifelian-D14	D14	390.82 ± 0.18	This paper	392.86 ± 0.42	392.86 ± 0.42	392.86 ± 0.42	45.74 ± 0.50	43.03 ± 0.50	41.37 ± 0.50
A-baseCarboniferous-D13	D13	394.290 ± 0.097	This paper	363.36 ± 0.86	363.36 ± 0.86	363.36 ± 0.86	100.00 ± 1.01	100.00 ± 0.52	100.00 ± 0.55
A-baseFamennian-D13	D13	394.290 ± 0.097	This paper	377.18 ± 0.84	377.18 ± 0.84	377.18 ± 0.84	73.19 ± 1.01	77.88 ± 0.52	80.23 ± 0.55
A-baseFrasnian-D13	D13	394.290 ± 0.097	This paper	383.88 ± 0.61	383.88 ± 0.61	383.88 ± 0.61	59.78 ± 1.01	60.54 ± 0.52	67.17 ± 0.55
A-baseGivetian-D13	D13	394.290 ± 0.097	This paper	388.79 ± 0.46	388.79 ± 0.46	388.79 ± 0.46	52.42 ± 1.01	52.19 ± 0.52	56.45 ± 0.55
A-baseEmsian-D6	D6	417.61 ± 0.12	McAdams et al. (2017)	411.53 ± 2.02	412.78 ± 1.54	410.57 ± 2.39	15.73 ± 1.52	19.28 ± 2.46	14.22 ± 1.13
A-basePragian-D6	D6	417.61 ± 0.12	McAdams et al. (2017)	413.23 ± 1.84	414.48 ± 1.32	412.27 ± 2.25	10.16 ± 1.52	13.96 ± 2.46	11.06 ± 1.13
A-baseLochkovian-D6	D6	417.61 ± 0.12	McAdams et al. (2017)	420.94 ± 1.40	422.18 ± 1.92	419.97 ± 1.00	0.00 ± 1.52	0.00 ± 2.46	0.00 ± 1.13
A-baseEmsian-D5	D5	417.68 ± 0.21	Husson et al. (2016)	411.60 ± 2.02	412.85 ± 1.56	410.64 ± 2.39	15.73 ± 1.52	19.28 ± 2.46	14.22 ± 1.13
A-basePragian-D5	D5	417.68 ± 0.21	Husson et al. (2016)	413.30 ± 1.85	414.55 ± 1.33	412.34 ± 2.25	10.16 ± 1.52	13.96 ± 2.46	11.06 ± 1.13
A-baseLochkovian-D5	D5	417.68 ± 0.21	Husson et al. (2016)	421.01 ± 1.41	422.24 ± 1.93	420.04 ± 1.02	0.00 ± 1.52	0.00 ± 2.46	0.00 ± 1.13

*Ages are based on anchored astrochronology durations extrapolated to each position of interest. Age uncertainty is 2σ.
†The units of scaled stratigraphic position are relative to the Silurian-Devonian boundary set equal to 0 and the Devonian-Carboniferous boundary set equal to 100. The uncertainty on scaled stratigraphic position is expressed as ± the half width.

See the Supplemental Material S1 for a detailed description of the way in which we assigned each age to a relative stratigraphic position. The abbreviations we use for each age (e.g., "D1") match those of the GTS2020. When available, we report age uncertainty as ± *X*(*Y*)[*Z*], where *X* is the internal or analytical uncertainty, *Y* is the uncertainty including the tracer calibration, and *Z* includes the decay constant uncertainty. For modeling, we used the *X* uncertainty for zircon dated using an EARTHTIME-calibrated isotope-dilution tracer (Condon et al., 2015; McLean et al., 2015), as the shared use of this SI-traceable reference material in time scale calibration eliminates this significant source of interlaboratory systematic errors. We used the *Y* uncertainty for legacy ages dated with an unknown or in-house tracer. For all legacy ages from GTS2020, any excess geologic scatter in the data was also accommodated into the age uncertainty. As all radioisotopic age constraints for our Devonian time scale utilized the same ^{238}U-^{206}Pb radioactive decay scheme, we can eliminate decay constant *Z* uncertainties while maintaining a self-consistent geochronological framework—a strategy that is more generally true for the entire Paleozoic.

Astrochronologic Constraints for Modeling

We incorporated astrochronologic constraints into our model by anchoring floating stage durations and uncertainties to radioisotopic ages (Fig. 4). Table 4 aggregates available astrochronologic constraints for Devonian stages and documents how we revised uncertainties in the stage durations (see Supplemental Material S1 for more detail on the astrochronologic studies and associated uncertainties). Astrochronology studies vary in terms of the sources of error that they incorporate into the duration uncertainty (Sinnesael et al., 2019), so our revised uncertainties incorporated at least one cycle-counting error as well as stratigraphic uncertainty in an attempt to standardize the uncertainties used in our modeling. When a stage had multiple published durations, we combined the durations into a weighted average (μ_{Stage}) using individual stage durations (μ_1, μ_2,…μ_n, where *n* is the number of individual cyclostratigraphy studies for a stage) weighted by our revised uncertainties (σ_1, σ_2,…σ_n, where *n* is the number of individual cyclostratigraphy studies for a stage) according to:

$$\mu_{Stage} = \frac{\frac{\mu_1}{(\sigma_1)^2} + \frac{\mu_2}{(\sigma_2)^2} + \ldots + \frac{\mu_n}{(\sigma_n)^2}}{\frac{1}{(\sigma_1)^2} + \frac{1}{(\sigma_2)^2} + \ldots + \frac{1}{(\sigma_n)^2}}. \quad (1)$$

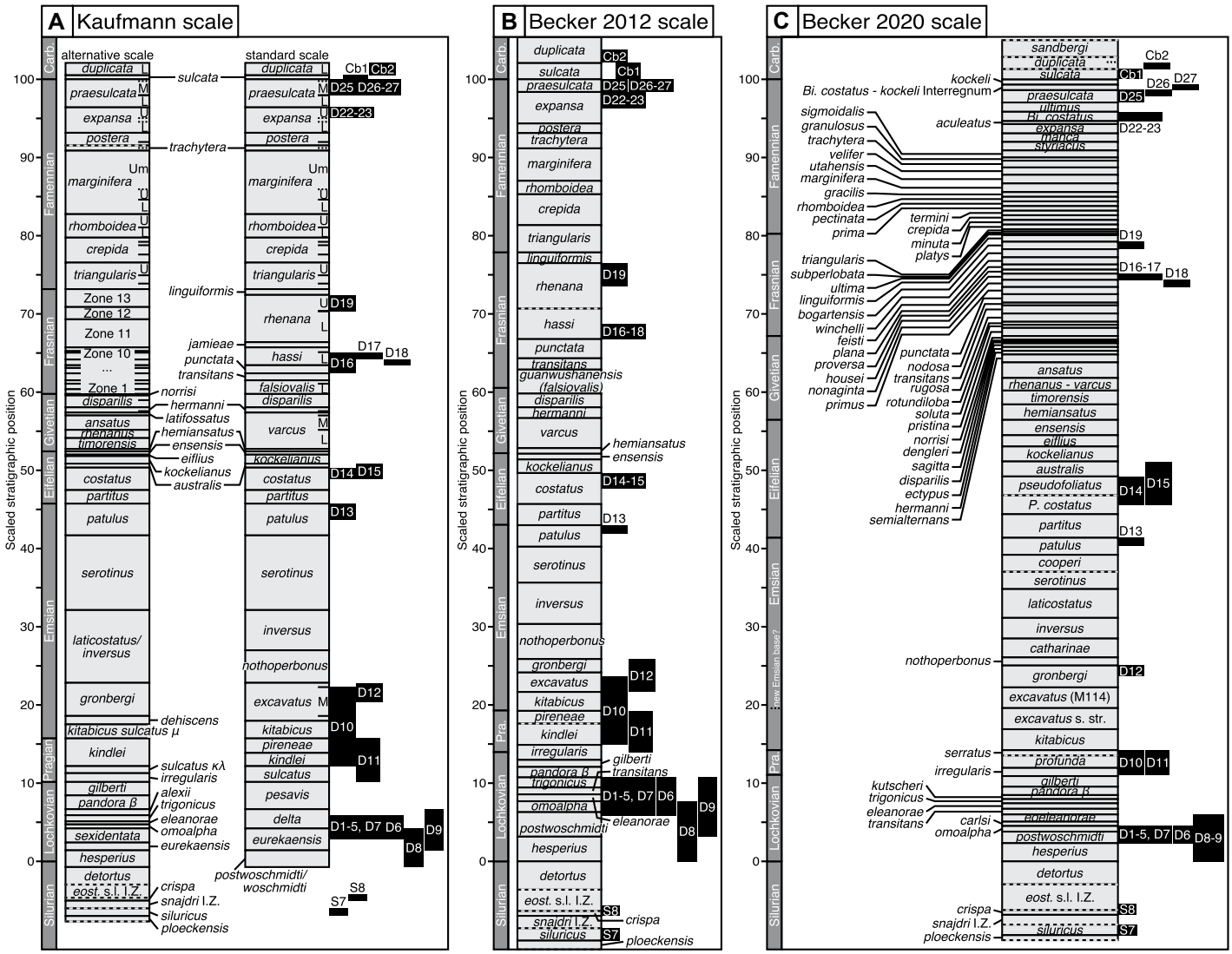

Figure 3. The three different starting biostratigraphic scales and the assigned position of the radioisotopic ages on those scales: (A) Kaufmann scale based on Kaufmann (2006), (B) Becker 2012 scale based on the Devonian chapter of the *Geologic Time Scale 2012* (Becker et al., 2012), and (C) Becker 2020 scale based on the Devonian chapter of the *Geologic Time Scale 2020* (Becker et al., 2020). The time scale (dark-gray rectangles) and the conodont biozone positions and scaling (light-gray rectangles) are reproduced from those references and scaled along the *y* axis (scaled stratigraphic position) such that each time scale ranges from 0 at the Silurian-Devonian boundary and 100 at the Devonian-Carboniferous boundary. The relative stratigraphic position of each dated volcanic layer is represented by the horizontal midpoint of the black rectangles, and the stratigraphic uncertainty is equal to ± the half-height of the black rectangles. The abbreviations we use for each age (i.e., "D1") matches that of the *Geologic Time Scale 2020*. Conodont genera as in references used to construct the different scales (Kaufmann 2006 and references therein; Becker et al., 2012, 2020; Aretz et al., 2020; Melchin et al., 2020). L—lower; M—middle; U—upper; Um—uppermost; Carb—Carboniferous; Pra—Pragian; M114—Morphotype 114; s. str.—sensu stricto; *eost—eosteinhornensis*; s.l.—sensu lato; I.Z.—interval zone; *Bi—Bispathodus*; *P—Polygnathus*.

We determined a combined uncertainty (σ_{Stage}) using the harmonic sum of the revised uncertainties for each duration as:

$$\sigma_{Stage} = \frac{1}{\frac{1}{(\sigma_1)^2} + \frac{1}{(\sigma_2)^2} + \ldots + \frac{1}{(\sigma_n)^2}}. \quad (2)$$

We used the combined duration and uncertainty for each stage, except for the Eifelian, where we used both the combined duration and uncertainty (Ellwood et al., 2015; combined with Pas et al., 2021) and the duration and revised uncertainty of Pas et al. (2021) as two separate astrochronologic constraints. Because we dated the Tioga B and Tioga F K-bentonites from within the same section studied by Pas et al. (2021), the Seneca Stone Quarry in New York, we could anchor the Pas et al. (2021) duration directly on radioisotopic dates for which the stratigraphic position within the section is known. This allowed us to compare how our anchoring and chaining process, described further below, varied between durations anchored

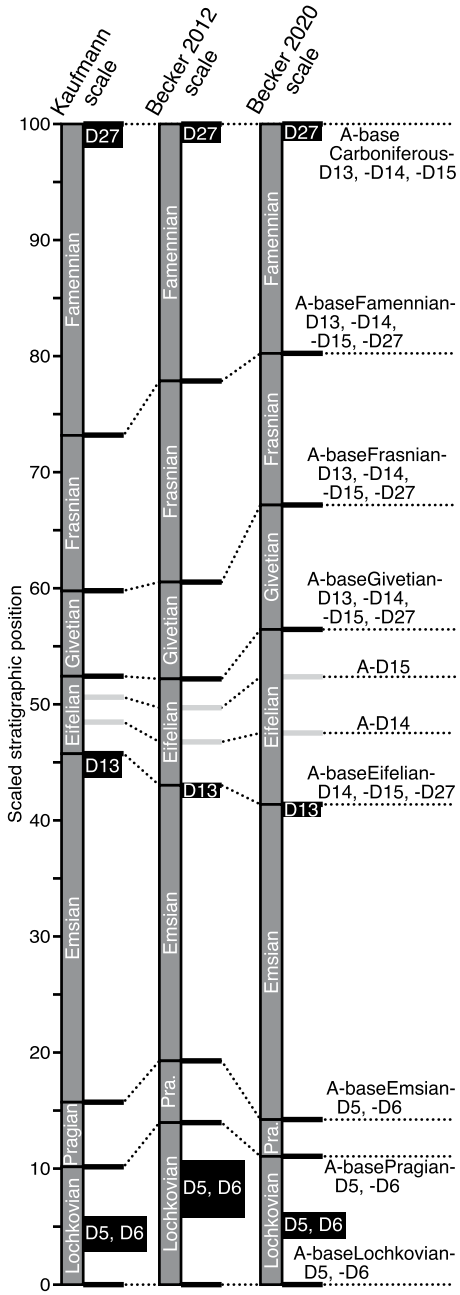

Figure 4. Scaled stratigraphic positions of the anchored astrochronologic constraints on each of the three starting time scales (Kaufmann, 2006; Becker et al., 2012, 2020) are shown as thick black lines and labeled to the right side of the figure. Floating stage durations and uncertainties are anchored on D5, D6, D13, or D27 (black rectangles with white labels) or A-D14 or A-D15 (thick gray lines). Dashed lines connect the position of each model input to its label on the right side of the figure. A-D14 and A-D15 function as both anchors and age constraints input into the model; see text for details. The uncertainty on D27 of the Becker et al. (2020) scale has been extended up to the Devonian-Carboniferous boundary for the purposes of anchoring astrochronology stage durations. Pra—Pragian.

on radioisotopic ages from the same section and combined durations anchored on radioisotopic ages from other sections. We used the astrochronologic constraints listed in Table 4 in our model for all three scales (Kaufmann, 2006; Becker et al., 2012, 2020), although uncertainty from the anchoring process caused each model to have unique astrochronologic inputs. To our knowledge, there is no astrochronology study on the duration of the Emsian Stage. The code used to do the astrochronology extrapolations is available as Supplemental Material S4. We indicate model inputs based on astrochronologic constraints with a prefix "A-", and the suffix on the astrochronologic constraints (e.g., "-D5") indicates the anchoring radioisotopic age. Table 5 shows the results of extrapolating the floating astrochronology durations to create inputs for the age-depth model.

To propagate the uncertainty in anchoring floating stage durations to radioisotopic ages, we used a Monte Carlo approach to sum the Gaussian error distributions of radioisotopic ages and uniform error distributions of astrochronology durations to extrapolate to the stage boundary of interest. We used the mean and standard deviation of the resulting summed distribution as the stage boundary age. We anchored the floating stage durations on ages D5, D6, D13, and D27 and used the combined astrochronology durations for each stage to chain up or down the time scale. Since ages D14 and D15 (Tioga B and Tioga F K-bentonites) are from the same section (Seneca Stone Quarry east of Fayette, New York) as some Eifelian cyclostratigraphy work (Pas et al., 2021), we built an additional astrochronology constraint into our model by using D14 and D15 as midstage anchors paired with the astrochronology duration determined on the same section. Because the scaled stratigraphic position of the Tioga B and Tioga F K-bentonites differed between the conodont biozone assignment and the position within the measured Eifelian section (Pas et al., 2021), we used A-D14 and A-D15 to indicate the radioisotopic ages of those K-bentonites at the measured stratigraphic positions, and we used D14 and D15 to indicate those radioisotopic ages at a scaled stratigraphic position corresponding to the conodont biozone assignment. For midstage anchors, we proportionally divided the astrochronology duration and uncertainty according to the relative stratigraphic position within the stage. See Supplemental Material S1 for a graphical explanation of this process.

We tied these extrapolated stage boundary ages to scaled stratigraphic positions based on the positions of the stage boundaries on each of the three conodont scales. We assigned a scaled stratigraphic uncertainty on the astrochronologic constraints according to the uncertainty on the anchoring position: a half width of 0.5 composite units for marker beds in a measured section and a half width equal to the conodont biozone half width for ages anchored to conodont biozones. For the Becker 2020 scale, we extended the stratigraphic position of D27 up to the Devonian-Carboniferous boundary, assuming that the Devonian-Carboniferous boundary lies within the uncertainty of the D27 age (Myrow et al., 2014).

Age-Depth Model Results

Entering the radioisotopic ages and astrochronologic constraints and their scaled stratigraphic positions into a Bayesian age-depth model using the modifiedBChron R package (Trayler et al., 2020) resulted in a modeled age and uncertainty for all stratigraphic positions on each of the three scales (Fig. 5). We report model ages as the median and the 95% highest density interval of the 10,000 iterations of the Markov chain Monte Carlo simulations. This creates a "beaded bracelet" pattern, where the uncertainty of the age model is smallest near well-constrained ages and increases where there are few or only poorly constrained ages, where the degree of constraint is determined by *both* the precision of the age and the precision of the placement of the age on the conodont biostratigraphic scale. The three conodont zonation schemes produced broadly similar age-depth models, particularly in the Early Devonian and near the Devonian-Carboniferous boundary. The model medians and 95% highest density intervals are least similar from ca. 390 to 368 Ma, suggesting the greatest discrepancy among the conodont biozonation schemes during this interval.

We rescaled each of the three age models, including the stages and the conodont biozones, according to the amount of offset between the median of the age-depth model and a linear projection (dotted line, Fig. 5) from the base of the Devonian to the base of the Carboniferous (Fig. 6). We compared the three revised scales after compressing and stretching the stages and conodont biozones from each scale (Fig. 6D) and found broad agreement between the three revised scales, particularly for the Middle to Late Devonian. Despite differences in the likelihoods input into the models, the age-depth modeling and linearization process produced remarkably

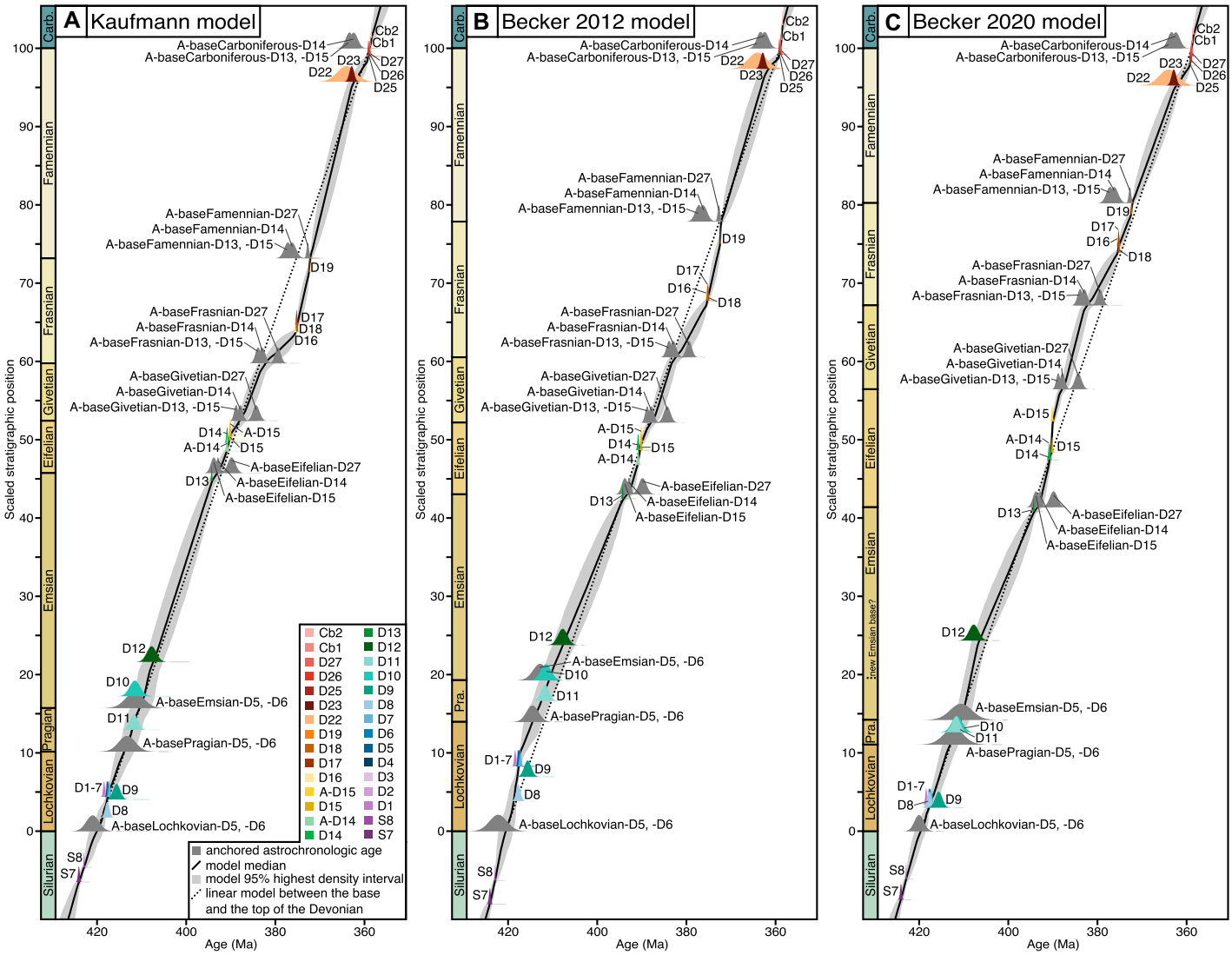

Figure 5. Age-depth model results for the (A) Kaufmann (2006) model, (B) Becker et al. (2012) model, and (C) Becker et al. (2020) model. The radioisotopic ages are shown as colored probability density functions, and the anchored astrochronologic constraints are shown as gray probability density functions. The model median is indicated by a solid black line, and the model 95% highest density interval is shown as a light-gray shaded region. A linear model from the base of the Devonian to the base of the Carboniferous is shown as a dotted line. Carb—Carboniferous; Pra—Pragian.

similar stages, both in terms of duration and absolute age. The ages and scaled stratigraphic positions of stage boundaries after modeling and linearization are given in Table 6.

DISCUSSION

New U-Pb Zircon Ages Aid in Improving the Devonian Time Scale

Our new ages for the Hercules I, Tioga B, and Tioga F K-bentonites improve the Devonian time scale by more precisely and accurately radioisotopically dating K-bentonites constrained within existing biostratigraphic frameworks. Our age for the Hercules I K-bentonite is more precise and older than the age of Kaufmann et al. (2005) (Fig. 7). They dated the tips of prismatic zircon grains and found a scattering of ages along the U-Pb concordia curve from 396.5 to 392.2 Ma, and they interpreted the youngest age of that cluster, 392.2 ± 1.5 Ma, as the eruption age of the K-bentonite (Kaufmann et al., 2005). Our weighted mean age on elongate, prismatic zircon grains from the Hercules I K-bentonite is 394.290 ± 0.097(0.21)[0.47] Ma, which falls within the range of oldest grains from Kaufmann et al. (2005). We believe our weighted mean age is a more robust eruption age for the K-bentonite because we chemically abraded the dated grains at 180 °C or 190 °C for 12 h in concentrated HF to eliminate Pb loss (modified from Mattinson, 2005), while Kaufmann et al. (2005) did a low-temperature (80 °C) leach in concentrated HF and HNO_3 for 2 h, which is likely insufficient to eliminate all Pb loss and therefore would bias their results to a younger age.

Similarly, we improved the age of the Tioga B K-bentonite by dating chemically abraded single zircon grains. Roden et al. (1990) dated multigrain monazite fractions from the Tioga B K-bentonite to avoid inheritance in zircon and determined a $^{207}Pb/^{235}U$ age of 390.0 ± 0.5 Ma. This age was recalculated to an equivalent $^{206}Pb/^{238}U$ age of 389.58 ± 0.86 Ma (including

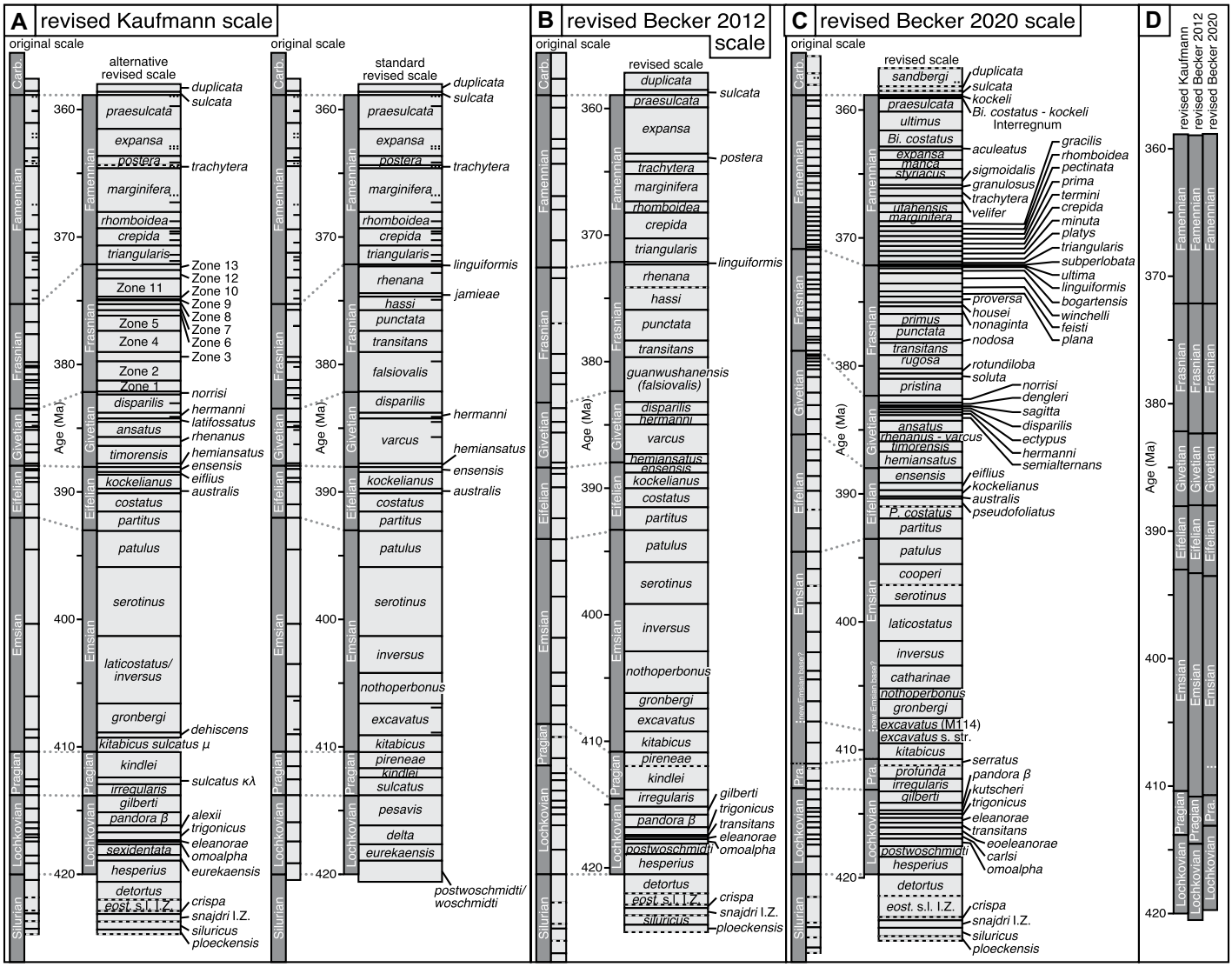

Figure 6. Revised conodont biozonation schemes as a result of linearizing the age-depth model to match relative stratigraphic position to numerical time: (A) Kaufmann (2006) alternative and standard scales; (B) Becker et al. (2012) scale; (C) Becker et al. (2020) scale. For each of the three biostratigraphic scales, the original time scale is shown on the left, and the revised stage (dark-gray rectangles) and conodont biozone (light-gray rectangles) heights are shown to the right of the original time scale. (D) Comparison of the revised stage heights for the three biostratigraphic scales. Conodont genera as in references used to construct the different scales (Kaufmann 2006 and references therein; Becker et al., 2012, 2020; Aretz et al., 2020; Melchin et al., 2020). Carb—Carboniferous; Pra—Pragian; M114—Morphotype 114; s. str.—sensu stricto; *eost—eosteinhornensis*; s.l.—sensu lato; I.Z.—interval zone; *Bi—Bispathodus*; *P—Polygnathus*.

decay constant uncertainty) for the GTS2012 (Schmitz, 2012). We mitigated the issue of inheritance by selecting needle-shaped zircon unlikely to have an inherited core, and we found the age of the Tioga B K-bentonite to be $390.82 \pm 0.18(0.26)[0.48]$ Ma, which is not only more precise but also without the systematic error amplification associated with using the ^{235}U-^{207}Pb chronometer.

To our knowledge, our work provides the first age for the Tioga F K-bentonite because Tucker et al. (1998) erroneously reported an age for the Tioga Middle Coarse Zone as the age of the Tioga F K-bentonite (Ver Straeten, 2004). Our weighted mean age of zircon from the Tioga F K-bentonite is $390.14 \pm 0.14(0.23)$ [0.47] Ma. The two Tioga K-bentonites have distinguishable ages that are consistent with their stratigraphic superposition. The resolution of these radioisotopic ages and the ability to temporally distinguish between them currently exceed our ability to biostratigraphically constrain the K-bentonites; however, the age-depth modeling, in its ability to leverage stratigraphic superposition, helps us to overcome the current limitations of biostratigraphic resolution. Accurate and precise ages and positions for the Tioga K-bentonites are critical for achieving a useful age-depth model through the Givetian, a stage without radioisotopic ages, because these K-bentonites are the dated events nearest to the Eifelian-Givetian boundary.

Anchoring Astrochronology Durations

We integrated astrochronologic constraints as likelihood functions in our Bayesian age-depth models by anchoring floating astrochronology durations on radioisotopic ages. In general, it is

TABLE 6. MODEL RESULTS: STAGE BOUNDARY AGES

Stage (or period) base	Kaufmann (2006) scale		Becker et al. (2012) scale		Becker et al. (2020) scale	
	Posterior age (Ma)	Scaled stratigraphic position†	Posterior age (Ma)	Scaled stratigraphic position†	Posterior age (Ma)	Scaled stratigraphic position†
Base of the Carboniferous	358.88 + 0.23/–0.23	100.00	358.96 + 0.20/–0.22	100.00	358.86 + 0.19/–0.19	100.00
Base of the Famennian	372.17 + 0.30/–0.48	73.17	372.15 + 0.23/–0.44	77.86	372.15 + 0.46/–0.46	80.24
Base of the Frasnian	382.19 + 1.52/–2.00	59.76	382.36 + 1.33/–1.59	60.54	382.31 + 1.08/–1.36	67.18
Base of the Givetian	388.06 + 1.04/–1.44	52.42	387.98 + 0.93/–1.27	52.19	387.95 + 0.82/–1.04	56.45
Base of the Eifelian	393.04 + 1.03/–1.31	45.75	393.31 + 0.84/–1.19	43.03	393.47 + 0.72/–0.99	41.38
Proposed base of the Emsian*	N.A.§	N.A.§	N.A.§	N.A.§	408.41 + 1.55/–1.67	19.58
Base of the Emsian	410.41 + 2.14/–2.44	15.73	410.84 + 2.17/–2.49	19.29	410.62 + 1.66/–1.95	14.22
Base of the Pragian	413.86 + 1.87/–2.18	10.16	414.55 + 1.92/–2.17	13.96	413.02 + 1.75/–1.91	11.06
Base of the Lochkovian	420.02 + 1.72/–1.51	0.00	420.52 + 1.64/–1.67	0.00	419.62 + 1.36/–1.14	0.00

*Proposed new Emsian base discussed in Becker et al. (2020).
†The units of scaled stratigraphic position are relative to the Silurian-Devonian boundary set equal to 0 and the Devonian-Carboniferous boundary set equal to 100.
§N.A.—not applicable.

not uncommon for studies to anchor astrochronology durations on a radioisotopic age from the same section (e.g., Da Silva et al., 2020; Pas et al., 2021) or on a time scale stage boundary age (e.g., Ma et al., 2020), but, to our knowledge, this is the first effort to chain multiple stage durations together for Bayesian modeling. Given the global distribution of Devonian ages and the scarcity of sections with both cyclostratigraphic and radioisotopic constraints, it can be difficult to pair astrochronologic constraints with radioisotopic age anchors. We managed this difficulty by providing the model with multiple astrochronology likelihoods and allowing the algorithm to determine the most probable age at a given scaled stratigraphic position. We anchored and chained together sequences of combined stage durations both forward and backward in time and repeated this process for multiple radioisotopic age anchors. This created multiple likelihood functions based on astrochronology at each stage boundary, providing our age-depth models with additional inputs beyond just radioisotopic ages. Adding astrochronology data improved our models because Bayesian age-depth models have improved precision as additional likelihood functions are added to the model (Blaauw et al., 2018).

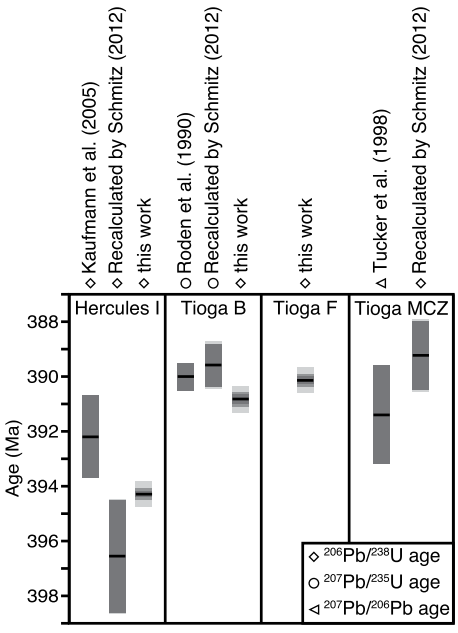

Figure 7. Comparison between new high-precision U-Pb zircon ages from this work and existing literature ages for the Hercules I, Tioga B, and Tioga F K-bentonites. Each age is indicated with a horizontal black line and surrounded by dark-, medium-, and light-gray rectangles that represent the 2σ analytical, analytical + tracer calibration, and analytical + tracer calibration + decay constant uncertainty, respectively. MCZ—Middle Coarse Zone cluster.

Additionally, we found that the anchoring and chaining process yielded similar likelihoods for combined durations anchored on radioisotopic ages near stage boundaries and for an individual duration (Eifelian Seneca Stone Quarry section; Pas et al., 2021) anchored on radioisotopic ages from K-bentonites within that section. For example, the likelihood probability density functions (PDFs) produced through anchoring on D13 (anchor near the stage boundary) and D15 (anchor within a section) overlapped with very similar mean ages and similar uncertainties (Fig. 5, see PDFs labeled "A-…-D13" and "A-…-D15"). This demonstrates the flexibility and reproducibility of our method of incorporating astrochronology durations into Bayesian modeling.

Integration of astrochronologic constraints as model likelihood data is a significant aspect of this work and differs from work done previously for time scale modeling. Rather than using astrochronology as likelihood functions, the Bayesian age-depth model of the Devonian by De Vleeschouwer and Parnell (2014) used astrochronology stage durations as rejection criteria to filter the posterior model results, subsampling the model runs that were in agreement with the Frasnian and Givetian durations available at the time. The resultant thinning of model runs leads to some concerns as to the recovery of the target stationary posterior distribution. Rather than integrating astrochronology and radioisotope geochronology, Baresel et al. (2017) discussed the results of their radioisotopic Bayesian age-depth models for the Permian-Triassic boundary in the context of existing astrochronological time scales to find both agreement and disagreement in terms of the duration of the extinction event, depending on which astrochronology data set was compared. Our approach conserves all well-mixed Markov chains and treats astrochronologic constraints as information the algorithm uses to generate the model, not just a way to evaluate a model generated by radioisotopic ages alone. Because Bayesian modeling can convolve disparate data sources, we can integrate and reconcile conflicting astrochronologic and radioisotopic data to produce a more robust age-depth model, rather than being left with potentially opposing astrochronology and radioisotopic time scale results.

Influence of Primary Conodont Biozone Scaling on the Time Scale

The Kaufmann (2006) and Becker et al. (2012, 2020) scales differ in the fundamental prior assumptions upon which the conodont biostratigraphic scales were constructed, with an assumption of either constant sedimentation rates in measured sections (Kaufmann, 2006) or equal biozone durations (Becker et al., 2012, 2020). Despite this difference, our Bayesian age-depth modeling process produced remarkably similar posterior scaled time scales. The age-depth models prior to linearization had overlapping 95% highest density intervals for most of the Devonian except for the late Eifelian through early Famennian (Fig. 5). During those times, the Kaufmann (2006) and Becker et al. (2012) age-depth models showed better agreement with each other than did either with the Becker et al.

(2020) age-depth model, suggesting that it is not the method of constructing the biostratigraphic scale (assumption of constant sedimentation rates or assumption of roughly equal biozone durations) that controls the age-depth modeling result, but rather the interpolation method for each scale that creates the relationship between zonal durations and numerical time.

The choice of the number of biozones to include in a conodont biozonation scheme has implications for the resulting age-depth model and how that conodont biozonation scheme is used by other workers. For the GTS2020, the number of conodont biozones in the Devonian grew to 85, up from 40 conodont biozones in the GTS2012 (Becker et al., 2012, 2020). Many of these additions occurred in the Late Devonian section. The addition of conodont biozones automatically shrank the average duration of conodont biozones. A consequence of shorter-duration conodont biozones is that a biostratigraphic constraint on an age within a particular biozone appears to be relatively more precise. For example, the duration of the *Caudicriodus postwoschmidti* zone was halved from the GTS2012 to the GTS2020, which means the precision of the relative stratigraphic height of an age assigned to this biozone similarly improved for the GTS2020 relative to the GTS2012. However, previous workers who paired a biostratigraphic constraint with an age may not have known the position of that age with such precision nor considered the biostratigraphic assignment with the newly added conodont biozones in mind, and thus the Becker et al. (2020) scale might have overestimated how well constrained those ages are in the biostratigraphic framework. Further, as additional biozones were added to the biozonation scheme, the absolute position of that age may also have changed, not just the precision, depending on how many biozones were added and where they were added. Most conodont biozones have been shifted to lower (older) relative stratigraphic positions on the Becker et al. (2020) scale relative to the Becker et al. (2012) scale, in some cases shifting to a position entirely below, with no overlap with the position on the Becker et al. (2012) scale (e.g., *Gondwania irregularis*, *Palmatolepis marginifera*). The modification of a conodont biozonation scheme is a natural result of more regional and global biostratigraphic studies, and improvements to conodont biozonation schemes should be embraced, but the discrepancies between the three biostratigraphic scales analyzed here emphasize the need for careful contextualization of dated volcanic layers so that radioisotopic ages can be applied accurately to future biostratigraphic scales.

The age-depth modeling process can be leveraged to examine and improve the consistency between the three biostratigraphic scales. When rescaled via their median Bayesian age-depth relationship, the agreement among the three models in terms of stage duration and numerical age is noteworthy (Fig. 6D). This convergence demonstrates that Bayesian age-depth modeling, particularly with the added step of time-linear rescaling, can produce robust time scales even with significant uncertainty in the relative stratigraphic positions of radioisotopic ages. The convergence on similar stage boundary ages for our three time scales, especially when compared to previous Devonian time scales (Fig. 8), suggests that model inputs that varied between the scales, namely, the starting conodont biozonation schemes and consequently the scaled stratigraphic positions of ages, are not an overly sensitive influence on the resulting time scales, perhaps because of the size of the scaled stratigraphic position uncertainty on each age (Supplemental Material S1). Thus, this modeling process allows us to manage our current limitations in biostratigraphic resolution and dampens the effects of variation between different conodont biozonation schemes.

Age-Depth Modeling and Future Time Scale Work

The ultimate goal of time scale modeling should be to produce an objective and reproducible time scale given the available data, not one that underestimates uncertainty for the sake of "improving" stage boundary ages by making them more precise without accompanying improvements in accuracy. Our age-depth models produced calibrated stage boundary ages with uncertainties ranging from 0.19 to 2.49 m.y. (Table 6), which quantitatively convolved both geochronologic and stratigraphic uncertainty. The calibrated stage boundary ages with the highest uncertainty and the portions of the age-depth model with the widest 95% highest density interval signal areas of the time scale to target for future work. For example, the ages of the bases of the Lochkovian, Pragian, and Emsian Stages have relatively high uncertainty that has not changed significantly with these new models (Fig. 8), largely because of the poor biostratigraphic control on radioisotopic ages. Nonetheless, the time scales derived from this study generally show more similarity to each other than they do to previous time scales or than previous time scales do to each other (Fig. 8).

Apart from creating newly calibrated time scales, this modeling process also prompted us to reflect on the quality of our model inputs. For example, radioisotopic ages D10–D12 have large stratigraphic and age uncertainties, and thus the model 95% highest density interval only slightly

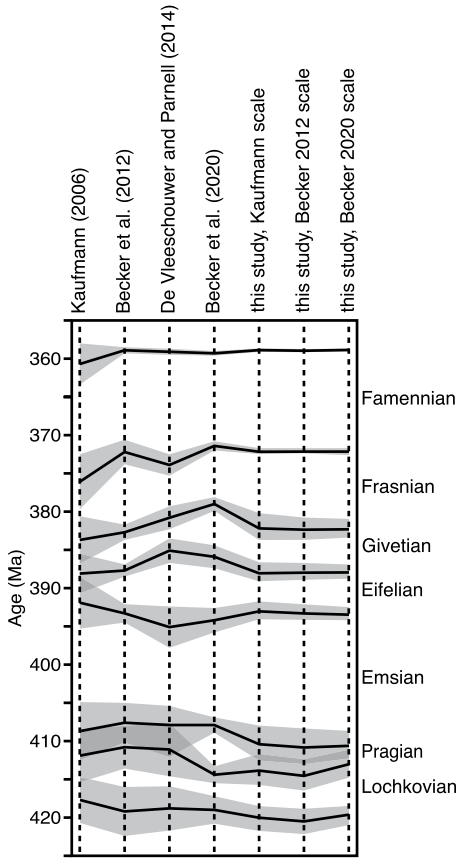

Figure 8. Comparison between stage boundary ages and uncertainties from this work and the previous literature. The vertical dashed lines represent a time scale, and the thick black lines represent the stage boundary age for each reference. The gray shaded region represents the stage boundary age uncertainty.

constricts at those events, since there is a large spread in positions that the algorithm can select to represent those events (Fig. 9). Better age precision may be achieved by redating some of these volcanic layers, but our ability to decrease relative stratigraphic uncertainty in our modeling may be limited by the actual lack of biotic variability during certain stages, particularly the Emsian (Brett et al., 2020). By contrast, the radioisotopic ages and conodont biozone assignments for D16–D18 are tightly constrained, so much so that the conodont zonal boundaries are within the resolution of the uncertainty on the radioisotopic ages, and the model 95% highest density interval in the Frasnian near D16–D18 is much more restricted than that in the Pragian and early Emsian near D10–D12 (Fig. 9). Further, the median of the age-depth model near D16–D18 requires a significant shift during the linearization process for the Kaufmann (2006) and Becker et al. (2012)

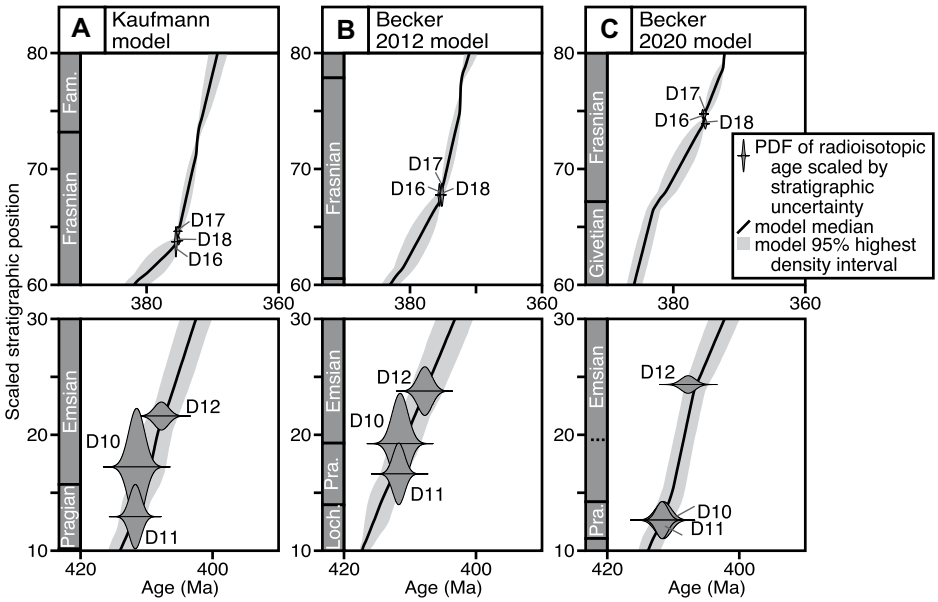

Figure 9. Age-depth model results for the (A) Kaufmann model, (B) Becker et al. (2012) model, and (C) Becker et al. (2020) model highlighting radioisotopic ages D16–D18 (top panels) and D10–D12 (bottom panels). Radioisotopic ages are shown as horizontally mirrored probability density functions (PDFs), where the height of the PDF is scaled to the uncertainty in stratigraphic position for that age. Fam—Famennian; Loch—Lochkovia; Pra—Pragian.

models, showing that for those models, tightly constrained radioisotopic ages can indicate where the time scale most strongly diverges from scaling with numerical time (Fig. 5).

The age-depth models also reveal shortcomings in the astrochronology ages input into the model. For the anchored astrochronology ages of the Middle and Late Devonian, the further they are extrapolated from their anchor point, generally the greater is the offset between the astrochronology age input and the linearized model position of that astrochronology age. For example, the astrochronology durations anchored on A-D14 and A-D15, the Tioga K-bentonites, have increasing horizontal offset from the linearized model with increasing scaled stratigraphic position (Fig. 5). This suggests that the astrochronology durations that are chained together to create extrapolated anchored astrochronology ages are systematically too short. This appears to indicate the potential for hiatuses and a bias for undercounting cycles, although there could be further issues of extrapolation and correlation to biotic events. Future work should target sections that contain global stage markers and/or completely span stages and include interspersed dateable volcanic layers.

CONCLUSIONS

(1) The Devonian time scale was improved in this work by dating key K-bentonites with greater precision and accuracy. The U-Pb zircon age of the Emsian Hercules I K-bentonite is $394.290 \pm 0.097(0.21)[0.47]$ Ma. The ages of the Eifelian Tioga B and Tioga F K-bentonites are $390.82 \pm 0.18(0.26)[0.48]$ Ma and $390.14 \pm 0.14(0.23)[0.47]$ Ma, respectively.

(2) A Bayesian age-depth modeling process managed the dissimilarities of different starting conodont biozonation schemes, incorporated radioisotopic ages, and integrated floating astrochronology durations to produce a robust calibration of the Devonian time scale. The age-depth models can be linearized to create a time scale scaled by numeric time, creating a time scale that is a useful template on which to contextualize and understand climatic, biotic, and stratigraphic proxies. These methods can be applied to improve the time scale for other periods, as well.

(3) The three linearized time scales (one for each starting conodont biozonation scheme) are remarkably similar, demonstrating that a probabilistic model can account for the differences in starting biostratigraphic scales, and lending confidence to the stage boundary ages produced by this modeling.

(4) The Bayesian age-depth models for the Kaufmann (2006) and Becker et al. (2012) scales show the most divergence from linearity during the Frasnian, suggesting that the prior biostratigraphic scales were most disassociated from the numerical time scale during that stage. By comparison, the Becker et al. (2020) model more closely matches linearity during the Frasnian, indicating that Frasnian modifications to the Becker et al. (2020) conodont biozonation scheme created a better match to numerical time. This shows how the process of Bayesian age-depth modeling is helpful in evaluating modifications to conodont biozonation schemes, and it demonstrates an approach for linking and comparing previously disconnected data sets.

(5) Bayesian age-depth modeling can inform targets for future time scale work. Our models demonstrate that the Devonian time scale would benefit from additional work refining the ages of the bases of the Lochkovian, Pragian, and Emsian Stages by acquiring radioisotopic ages with better stratigraphic position control. Currently dated volcanic layers from the Pragian and early Emsian generally have significant uncertainty and therefore exert minimal influence on the model, so future work could redate these volcanic layers with increased precision or seek out similarly positioned volcanic layers to add to the time scale.

ACKNOWLEDGMENTS

This project was supported through a collaborative grant from the National Science Foundation (NSF) Sedimentary Geology and Paleobiology Program (EAR-1124275, EAR-1124488). Vladimir I. Davydov was partially supported by a grant from the Russian Scientific Foundation (19-17-00178). Funding for the analytical infrastructure of the Boise State Isotope Geology Laboratory was provided by NSF Major Research Instrumentation grants EAR-0521221 and EAR-1337887, and NSF EAR Instrumentation and Facilities Program grant EAR-0824974. Manfred Gereke and Eberhard Schindler provided local geological expertise and access to the Wetteldorf section. We thank Editors Brad Singer and Brad Cramer for their handling of the manuscript and David De Vleeschouwer and an anonymous reviewer for their constructive feedback. We are particularly grateful to David De Vleeschouwer for compiling Table 4 and assisting us in combining astrochronology durations for use in our modeling.

REFERENCES CITED

Algeo, T.J., and Scheckler, S.E., 2010, Land plant evolution and weathering rate changes in the Devonian: Journal of Earth Science, v. 21, p. 75–78, https://doi.org/10.1007/s12583-010-0173-2.

Aretz, M., Herbig, H.G., Wang, X.D., Gradstein, F.M., Agterberg, F.P., and Ogg, J.G., 2020, The Carboniferous Period, *in* Gradstein, F.M., Ogg, J.G., Schmitz, M.D., and Ogg, G.M., eds., Geologic Time Scale 2020: Amsterdam, Netherlands, Elsevier, p. 811–874, https://doi.org/10.1016/B978-0-12-824360-2.00023-1.

Averbuch, O., Tribovillard, N., De Vleeschouwer, X., Riquier, L., Mistiaen, B., and Vliet-Lanoe, B.V., 2005, Mountain building–enhanced continental weathering and organic carbon burial as major causes for climatic cooling at the Frasnian-Famennian boundary (c. 376 Ma)?: Terra Nova, v. 17, p. 25–34, https://doi.org/10.1111/j.1365-3121.2004.00580.x.

Baresel, B., Bucher, H., Brosse, M., Cordey, F., Guodun, K., and Schaltegger, U., 2017, Precise age for the Permian-Triassic boundary in South China from high-precision

U-Pb geochronology and Bayesian age-depth modeling: Solid Earth, v. 8, p. 361–378, https://doi.org/10.5194/se-8-361-2017.

Becker, R.T., Gradstein, F.M., and Hammer, O., 2012, The Devonian Period, *in* Gradstein, F.M., Ogg, J.G., Schmitz, M.D., and Ogg, G.M., eds., The Geologic Time Scale 2012: Amsterdam, Netherlands, Elsevier BV, p. 559–601, https://doi.org/10.1016/B978-0-444-59425-9.00022-6.

Becker, R.T., Marshall, J.E.A., Da Silva, A.-C., Agterberg, F.P., Gradstein, F.M., and Ogg, J.G., 2020, The Devonian Period, *in* Gradstein, F.M., Ogg, J.G., Schmitz, M.D., and Ogg, G.M., eds., Geologic Time Scale 2020: Amsterdam, Netherlands, Elsevier, p. 733–810, https://doi.org/10.1016/B978-0-12-824360-2.00022-X.

Blaauw, M., Christen, J.A., Bennett, K.D., and Reimer, P.J., 2018, Double the dates and go for Bayes—Impacts of model choice, dating density and quality on chronologies: Quaternary Science Reviews, v. 188, p. 58–66, https://doi.org/10.1016/j.quascirev.2018.03.032.

Bodorkos, S., Pogson, D., and Friedman, R., 2017, Zircon U-Pb dating of biostratigraphically constrained felsic volcanism in the Lachlan orogen via SHRIMP and CA-IDTIMS: Implications for the division of Early Devonian time [abs.], *in* Vearncombe, J., ed., Bulletin No. 65: Granites2017@Benalla: Australia, Australian Institute of Geoscientists, p. 11–14.

Brett, C.E., and Ver Straeten, C.A., 1994, Stratigraphy and facies relationships of the Eifelian Onondaga Limestone (Middle Devonian) in western and west central New York State, *in* Brett, C.E., and Scatterday, J., eds., 66th Annual Meeting Guidebook: Rochester, New York, New York State Geological Association, p. 221–269.

Brett, C.E., Zambito, J.J., McLaughlin, P.I., and Emsbo, P., 2020, Revised perspectives on Devonian biozonation and environmental volatility in the wake of recent timescale revisions: Palaeogeography, Palaeoclimatology, Palaeoecology, v. 549, 108843, https://doi.org/10.1016/j.palaeo.2018.06.037.

Brocke, R., Fatka, O., Lindemann, R.H., Schindler, E., and Ver Straeten, C.A., 2016, Palynology, dacryoconarids and the lower Eifelian (Middle Devonian) basal Chotec event: Case studies from the Prague and Appalachian Basins, *in* Becker, R.T., Königshof, P., and Brett, C.E., eds., Devonian Climate, Sea Level and Evolutionary Events: Geological Society [London] Special Publication 423, p. 123–169, https://doi.org/10.1144/SP423.8.

Condon, D.J., Schoene, B., McLean, N.M., Bowring, S.A., and Parrish, R.R., 2015, Metrology and traceability of U-Pb isotope dilution geochronology (EARTHTIME tracer calibration Part I): Geochimica et Cosmochimica Acta, v. 164, p. 464–480, https://doi.org/10.1016/j.gca.2015.05.026.

Cramer, B.D., Schmitz, M.D., Huff, W.D., and Bergström, S.M., 2014, High-precision U-Pb zircon age constraints on the duration of rapid biogeochemical events during the Ludlow Epoch (Silurian Period): Journal of the Geological Society [London], v. 172, p. 157–160, https://doi.org/10.1144/jgs2014-094.

Da Silva, A.-C., Hladil, J., Chadimová, L., Slavík, L., Hilgen, F.J., Bábek, O., and Dekkers, M.J., 2016, Refining the Early Devonian time scale using Milankovitch cyclicity in Lochkovian–Pragian sediments (Prague synform, Czech Republic): Earth and Planetary Science Letters, v. 455, p. 125–139, https://doi.org/10.1016/j.epsl.2016.09.009.

Da Silva, A.-C., Sinnesael, M., Claeys, P., Davies, J.H.F.L., de Winter, N.J., Percival, L.M.E., Schaltegger, U., and Vleeschouwer, D.D., 2020, Anchoring the Late Devonian mass extinction in absolute time by integrating climatic controls and radio-isotopic dating: Scientific Reports, v. 10, 12940, https://doi.org/10.1038/s41598-020-69097-6.

Davydov, V.I., Crowley, J.L., Schmitz, M.D., and Poletaev, V.I., 2010, High-precision U-Pb zircon age calibration of the global Carboniferous time scale and Milankovitch band cyclicity in the Donets Basin, eastern Ukraine: Geochemistry Geophysics Geosystems, v. 11, Q0AA04, https://doi.org/10.1029/2009GC002736.

Davydov, V., Schmitz, M.D., and Korn, D., 2011, The Hangenberg event was abrupt and short at the global scale: The quantitative integration and intercalibration of biotic and geochronologic data within the Devonian-Carboniferous transition: Geological Society of America Abstracts with Programs, v. 43, no. 5, p. 128, https://gsa.confex.com/gsa/2011AM/webprogram/Paper195211.html.

De Vleeschouwer, D., and Parnell, A.C., 2014, Reducing time-scale uncertainty for the Devonian by integrating astrochronology and Bayesian statistics: Geology, v. 42, p. 491–494, https://doi.org/10.1130/G35618.1.

De Vleeschouwer, D., Whalen, M.T., Day, J.E., and Claeys, P., 2012, Cyclostratigraphic calibration of the Frasnian (Late Devonian) time scale (western Alberta, Canada): Geological Society of America Bulletin, v. 124, p. 928–942, https://doi.org/10.1130/B30547.1.

De Vleeschouwer, D., Boulvain, F., Da Silva, A.-C., Pas, D., Labaye, C., and Claeys, P.F., 2013a, The astronomical calibration of the Givetian (Middle Devonian) time scale (Dinant synclinorium, Belgium): San Francisco, California, American Geophysical Union, Fall Meeting supplement, abstract GP43A–1184.

De Vleeschouwer, D., Rakociński, M., Racki, G., Bond, D.P.G., Sobień, K., and Claeys, P., 2013b, The astronomical rhythm of Late Devonian climate change (Kowala section, Holy Cross Mountains, Poland): Earth and Planetary Science Letters, v. 365, p. 25–37, https://doi.org/10.1016/j.epsl.2013.01.016.

De Vleeschouwer, D., Boulvain, F., Da Silva, A.-C., Pas, D., Labaye, C., and Claeys, P., 2015, The astronomical calibration of the Givetian (Middle Devonian) time scale (Dinant synclinorium, Belgium): Geological Society [London] Special Publication 414, p. 245–256, https://doi.org/10.1144/SP414.3.

Ellwood, B.B., Tomkin, J.H., Hassani, A.E., Bultynck, P., Brett, C.E., Schindler, E., Feist, R., and Bartholomew, A.J., 2011, A climate-driven model and development of a floating point time scale for the entire Middle Devonian Givetian Stage: A test using magnetostratigraphy susceptibility as a climate proxy: Palaeogeography, Palaeoclimatology, Palaeoecology, v. 304, p. 85–95, https://doi.org/10.1016/j.palaeo.2010.10.014.

Ellwood, B.B., El Hassani, A., Tomkin, J.H., and Bultynck, P., 2015, A climate-driven model using time-series analysis of magnetic susceptibility (χ) datasets to represent a floating-point high-resolution geological timescale for the Middle Devonian Eifelian Stage: Geological Society [London] Special Publication 414, p. 209–223, https://doi.org/10.1144/SP414.4.

Ernst, R.E., Rodygin, S.A., and Grinev, O.M., 2020, Age correlation of large igneous provinces with Devonian biotic crises: Global and Planetary Change, v. 185, 103097, https://doi.org/10.1016/j.gloplacha.2019.103097.

Gordon, G.W., Rockman, M., Turekian, K.K., and Over, J., 2009, Osmium isotopic evidence against an impact at the Frasnian-Famennian boundary: American Journal of Science, v. 309, p. 420–430, https://doi.org/10.2475/05.2009.03.

Gradstein, F.M., Ogg, J.G., Schmitz, M.D., and Ogg, G.M., eds., 2012, Geologic Time Scale 2012: Amsterdam, Netherlands, Elsevier, 1176 p., https://doi.org/10.1016/c2011-1-08249-8.

Gradstein, F.M., Ogg, J.G., Schmitz, M.D., and Ogg, G.M., eds., 2020, Geologic Time Scale 2020: Amsterdam, Netherlands, Elsevier, 1390 p., https://doi.org/10.1016/c2020-1-02369-3.

Haslett, J., and Parnell, A.C., 2008, A simple monotone process with application to radiocarbon-dated depth chronologies: Applied Statistics, v. 57, p. 399–418, https://doi.org/10.1111/j.1467-9876.2008.00623.x.

House, M.R., 1995, Devonian precessional and other signatures for establishing a Givetian timescale, *in* House, M.R., and Gale, A.S., eds., Orbital Forcing Timescales and Cyclostratigraphy: Geological Society [London] Special Publication 85, p. 37–49, https://doi.org/10.1144/GSL.SP.1995.085.01.03.

House, M.R., 2002, Strength, timing, setting and cause of mid-Palaeozoic extinctions: Palaeogeography, Palaeoclimatology, Palaeoecology, v. 181, p. 5–25, https://doi.org/10.1016/S0031-0182(01)00471-0.

House, M.R., and Gradstein, F.M., 2004, The Devonian Period, *in* Ogg, J.G., Gradstein, F.M., and Smith, A.G., eds., A Geologic Time Scale 2004: Cambridge, UK, Cambridge University Press, p. 202–221, https://doi.org/10.1017/CBO9780511536045.015.

Husson, J.M., Schoene, B., Bluher, S., and Maloof, A.C., 2016, Chemostratigraphic and U-Pb geochronologic constraints on carbon cycling across the Silurian-Devonian boundary: Earth and Planetary Science Letters, v. 436, p. 108–120, https://doi.org/10.1016/j.epsl.2015.11.044.

Jaffey, A.H., Flynn, K.F., Glendenin, L.E., Bentley, W.T., and Essling, A.M., 1971, Precision measurement of half-lives and specific activities of ^{235}U and ^{238}U: Physical Review C, v. 4, p. 1889–1906, https://doi.org/10.1103/PhysRevC.4.1889.

Kaufmann, B., 2006, Calibrating the Devonian time scale: A synthesis of U-Pb ID-TIMS ages and conodont stratigraphy: Earth-Science Reviews, v. 76, p. 175–190, https://doi.org/10.1016/j.earscirev.2006.01.001.

Kaufmann, B., Trapp, E., Mezger, K., and Weddige, K., 2005, Two new Emsian (Early Devonian) U-Pb zircon ages from volcanic rocks of the Rhenish Massif (Germany): Implications for the Devonian time scale: Journal of the Geological Society [London], v. 162, p. 363–371, https://doi.org/10.1144/0016-764904-012.

Kiessling, W., 2008, Sampling-standardized expansion and collapse of reef building in the Phanerozoic: Fossil Record (Weinheim), v. 11, p. 7–18, https://doi.org/10.5194/fr-11-7-2008.

Kiessling, W., and Simpson, C., 2011, On the potential for ocean acidification to be a general cause of ancient reef crises: Global Change Biology, v. 17, p. 56–67, https://doi.org/10.1111/j.1365-2486.2010.02204.x.

Klapper, G., 1971, Sequence within the conodont genus *Polygnathus* in the New York lower Middle Devonian: Geologica et Palaeontologica, v. 5, p. 59–79.

Klapper, G., 1981, Review of New York Devonian conodont biostratigraphy, *in* Oliver, W.A., Jr., and Klapper, G., eds., Devonian Biostratigraphy of New York: Binghampton, New York, International Union of Geological Sciences Subcommission on Devonian Stratigraphy, p. 57–66.

Klapper, G., and Oliver, W.A., Jr., 1995, The Detroit River Group is Middle Devonian: Discussion on "Early Devonian age of the Detroit River Group, inferred from Arctic stromatoporoids": Canadian Journal of Earth Sciences, v. 32, p. 1070–1073, https://doi.org/10.1139/e95-088.

Klapper, G., Ziegler, W., and Mashkova, T.V., 1978, Conodonts and correlation of Lower-Middle Devonian boundary beds in the Barrandian area of Czechoslovakia: Geologica et Palaeontologica, v. 12, p. 103–116.

Krogh, T.E., 1973, A low-contamination method for hydrothermal decomposition of zircon and extraction of U and Pb for isotopic age determinations: Geochimica et Cosmochimica Acta, v. 37, p. 485–494, https://doi.org/10.1016/0016-7037(73)90213-5.

Lanik, A., Over, D.J., Schmitz, M., and Kirchgasser, W.T., 2016, Testing the limits of chronostratigraphic resolution in the Appalachian Basin, Late Devonian (middle Frasnian), eastern North America: New U-Pb zircon dates for the Belpre Tephra suite: Geological Society of America Bulletin, v. 128, p. 1813–1821, https://doi.org/10.1130/B31408.1.

Ma, K., Hinnov, L.A., Zhang, X., and Gong, Y., 2020, Astronomical time calibration of the Upper Devonian Lali section, South China: Global and Planetary Change, v. 193, 103267, https://doi.org/10.1016/j.gloplacha.2020.103267.

Mattinson, J.M., 2005, Zircon U-Pb chemical abrasion ("CA-TIMS") method: Combined annealing and multi-step partial dissolution analysis for improved precision and accuracy of zircon ages: Chemical Geology, v. 220, p. 47–66, https://doi.org/10.1016/j.chemgeo.2005.03.011.

McAdams, N.E.B., Schmitz, M.D., Kleffner, M.A., Verniers, J., Vandenbroucke, T.R.A., Ebert, J.R., and Cramer, B.D., 2017, A new, high-precision CA-ID-TIMS date for the 'Kalkberg' K-bentonite (Judds Falls Bentonite): Lethaia, v. 51, p. 344–356, https://doi.org/10.1111/let.12241.

McLean, N.M., Condon, D.J., Schoene, B., and Bowring, S.A., 2015, Evaluating uncertainties in the calibration of isotopic reference materials and multi-element

isotopic tracers (EARTHTIME tracer calibration part II): Geochimica et Cosmochimica Acta, v. 164, p. 481–501, https://doi.org/10.1016/j.gca.2015.02.040.

Melchin, M.J., Sadler, P.M., and Cramer, B.D., 2020, The Silurian Period, *in* Gradstein, F.M., Ogg, J.G., Schmitz, M.D., and Ogg, G.M., eds., Geologic Time Scale 2020: Amsterdam, Netherlands, Elsevier, p. 695–732, https://doi.org/10.1016/B978-0-12-824360-2.00021-8.

Myrow, P.M., Ramezani, J., Hanson, A.E., Bowring, S.A., Racki, G., and Rakociński, M., 2014, High-precision U-Pb age and duration of the latest Devonian (Famennian) Hangenberg event, and its implications: Terra Nova, v. 26, p. 222–229, https://doi.org/10.1111/ter.12090.

Parnell, A.C., Haslett, J., Allen, J.R., Buck, C.E., and Huntley, B., 2008, A flexible approach to assessing synchroneity of past events using Bayesian reconstructions of sedimentation history: Quaternary Science Reviews, v. 27, p. 1872–1885, https://doi.org/10.1016/j.quascirev.2008.07.009.

Parry, S.F., Noble, S.R., Crowley, Q.G., and Wellman, C.H., 2011, A high-precision U-Pb age constraint on the Rhynie Chert Konservat-Lagerstätte: Time scale and other implications: Journal of the Geological Society [London], v. 168, p. 863–872, https://doi.org/10.1144/0016-76492010-043.

Pas, D., Hinnov, L., Day, J.E., Kodama, K., Sinnesael, M., and Liu, W., 2018, Cyclostratigraphic calibration of the Famennian Stage (Late Devonian, Illinois Basin, USA): Earth and Planetary Science Letters, v. 488, p. 102–114, https://doi.org/10.1016/j.epsl.2018.02.010.

Pas, D., Da Silva, A.-C., Over, D.J., Brett, C.E., Brandt, L., Over, J.-S., Hilgen, F.J., and Dekkers, M.J., 2021, Cyclostratigraphic calibration of the Eifelian Stage (Middle Devonian, Appalachian Basin, western New York, USA): Geological Society of America Bulletin, v. 133, p. 277–286, https://doi.org/10.1130/B35589.1.

Percival, L.M.E., Davies, J.H.F.L., Schaltegger, U., De Vleeschouwer, D., Da Silva, A.-C., and Föllmi, K.B., 2018, Precisely dating the Frasnian-Famennian boundary: Implications for the cause of the Late Devonian mass extinction: Scientific Reports, v. 8, 9578, https://doi.org/10.1038/s41598-018-27847-7.

R Core Team, 2020, R: A Language and Environment for Statistical Computing: Vienna, Austria, R Foundation for Statistical Computing, https://www.R-project.org/ (accessed July 2021).

Reimold, W.U., Kelley, S.P., Sherlock, S.C., Henkel, H., and Koeberl, C., 2005, Laser argon dating of melt breccias from the Siljan impact structure, Sweden: Implications for a possible relationship to Late Devonian extinction events: Meteoritics & Planetary Science, v. 40, p. 591–607, https://doi.org/10.1111/j.1945-5100.2005.tb00965.x.

Retallack, G.J., and Huang, C., 2011, Ecology and evolution of Devonian trees in New York, USA: Palaeogeography, Palaeoclimatology, Palaeoecology, v. 299, p. 110–128, https://doi.org/10.1016/j.palaeo.2010.10.040.

Roden, M.K., Parrish, R.R., and Miller, D.S., 1990, The absolute age of the Eifelian Tioga Ash Bed, Pennsylvania: The Journal of Geology, v. 98, p. 282–285, https://doi.org/10.1086/629399.

Schmitz, M.D., 2012, Appendix 2—Radiometric ages used in GTS2012, *in* Gradstein, F.M., Ogg, J.G., Schmitz, M.D., and Ogg, G.M., eds., The Geologic Time Scale 2012: Amsterdam, Netherlands, Elsevier BV, p. 1045–1082, https://doi.org/10.1016/B978-0-444-59425-9.15002-4.

Schmitz, M.D., and Schoene, B., 2007, Derivation of isotope ratios, errors, and error correlations for U-Pb geochronology using ^{205}Pb-^{235}U-(^{233}U)–spiked isotope dilution thermal ionization mass spectrometric data: Geochemistry Geophysics Geosystems, v. 8, Q08006, https://doi.org/10.1029/2006GC001492.

Sinnesael, M., et al., 2019, The Cyclostratigraphy Intercomparison Project (CIP): Consistency, merits and pitfalls: Earth-Science Reviews, v. 199, 102965, https://doi.org/10.1016/j.earscirev.2019.102965.

Smith, R.C., and Way, J.H., 1983, The Tioga Ash Beds at Selinsgrove Junction, *in* Nickelsen, R.P., and Cotter, E., eds., Silurian Depositional History and Alleghenian Deformation in the Pennsylvania Valley and Ridge: 48th Annual Field Conference of Pennsylvania Geologists: Danville, Pennsylvania, Field Conference of Pennsylvania Geologists, p. 74–88.

Stacey, J.S., and Kramers, J.D., 1975, Approximation of terrestrial lead isotope evolution by a two-stage model: Earth and Planetary Science Letters, v. 26, p. 207–221, https://doi.org/10.1016/0012-821X(75)90088-6.

Telford, R.J., Heegaard, E., and Birks, H.J.B., 2004, All age-depth models are wrong: But how badly?: Quaternary Science Reviews, v. 23, p. 1–5, https://doi.org/10.1016/j.quascirev.2003.11.003.

Trayler, R.B., Schmitz, M.D., Cuitiño, J.I., Kohn, M.J., Bargo, M.S., Kay, R.F., Strömberg, C.A.E., and Vizcaíno, S.F., 2020, An improved approach to age-modeling in deep time: Implications for the Santa Cruz Formation, Argentina: Geological Society of America Bulletin, v. 132, p. 233–244, https://doi.org/10.1130/B35203.1.

Tucker, R.D., Bradley, D.C., Ver Straeten, C.A., Harris, A.G., Ebert, J.R., and McCutcheon, S.R., 1998, New U-Pb zircon ages and the duration and division of Devonian time: Earth and Planetary Science Letters, v. 158, p. 175–186, https://doi.org/10.1016/S0012-821X(98)00050-8.

Ver Straeten, C.A., 2004, K-bentonites, volcanic ash preservation, and implications for Early to Middle Devonian volcanism in the Acadian orogen, eastern North America: Geological Society of America Bulletin, v. 116, p. 474–489, https://doi.org/10.1130/B25244.1.

Ver Straeten, C.A., 2007, Basinwide stratigraphic synthesis and sequence stratigraphy, upper Pragian, Emsian and Eifelian Stages (Lower to Middle Devonian), Appalachian Basin, *in* Becker, R.T., and Kirchgasser, W.T., eds., Devonian Events and Correlations: Geological Society [London] Special Publication 278, p. 39–81, https://doi.org/10.1144/SP278.3.

Way, J.H., Smith, R.C., and Roden, M.K., 1986, Detailed correlations across 175 miles of the Valley and Ridge of Pennsylvania using 7 ash beds in the Tioga zone, *in* Sevon, W.D., ed., Selected Geology of Bedford and Huntington Counties: 51st Annual Field Conference of Pennsylvania Geologists: Huntington, Pennsylvania, Field Conference of Pennsylvania Geologists, p. 55–72.

Weddige, K., 1977, Die Conodonten der Eifel-Stufe im Typusgebiet und inbenachbarten Faziesgebieten: Senckenbergiana Lethaea, v. 58, p. 271–419.

Weddige, K., 1982, The Wetteldorf Richtschnitt as boundary stratotype from the view point of conodont stratigraphy, *in* Ziegler, W., and Werner, R., eds., On Devonian Stratigraphy and Palaeontology of the Ardenno-Rhenish Mountains and Related Devonian Matters: Courier Forschungsinstitut Senckenberg, v. 55, p. 26–37.

Werner, R., and Winter, J., 1975, Bentonit-Horizonte im Grenzbereich Unterdevon/Mitteldevon in den Eifeler Richtschnitten: Senckenbergiana Lethaea, v. 56, p. 335–364.

Whalen, M.T., De Vleeschouwer, D., Payne, J.H., Day, J.E., Over, D.J., and Claeys, P., 2016, Pattern and timing of the Late Devonian biotic crisis in western Canada: Insights from carbon isotopes and astronomical calibration of magnetic susceptibility data, *in* Playton, T.E., Kerans, C., and Weissenberger, J.A.W., eds., New Advances in Devonian Carbonates: Outcrop Analogs, Reservoirs, and Chronostratigraphy: Society for Sedimentary Geology (SEPM) Special Publication 107, p. 185–201, https://doi.org/10.2110/sepmsp.107.02.

Ziegler, W., and Klapper, G., 1985, Stages of the Devonian System: Episodes, v. 8, p. 104–109, https://doi.org/10.18814/epiiugs/1985/v8i2/006.

Ziegler, W., and Werner, R., eds., 1982, On Devonian Stratigraphy and Palaeontology of the Ardenno-Rhenish Mountains and Related Devonian Matters: Courier Forschungsinstitut Senckenberg, v. 55, p. 498.

Science Editor: Brad S. Singer
Associate Editor: Bradley Cramer

Manuscript Received 23 March 2021
Revised Manuscript Received 2 July 2021
Manuscript Accepted 14 September 2021

Printed in the USA